People's Democratic Republic of Algeria

Ministry of Higher Education and Scientific Research

Kasdi Merbah University Ouargla

Faculty of Mathematics and Matter Sciences

Department of Physics

Master Thesis for the Academic Degree in Physics

Field: Matter Sciences

Specialty: Physics of Materials

Prepared by the student: Aliaa Guettaf

Title:

Study of physical properties of the lutetium hydride in β phase based the density functional theory

2025/06/04

In front of the jury panel composed of:

Omar Bentouila	Jury President	Kasdi Merbah Ouargla
Abdellatif Mamanou	Examiner	Kasdi Merbah Ouargla
Zahia Ayat	Supervisor	Kasdi Merbah Ouargla

Academic year: 2024/2025

Dedication

بسم الله الرحمن الرحيم

"وما تقدموا لأنفسكم من خيرٍ تجدوه عند الله هو خيرًا وأعظم أجرًا"

(Surah Al-Muzzammil, 20)

In the name of Allah, the Most Gracious, the Most Merciful

To the One to whom words ascend, intentions are weighed, and deeds are offered…

I dedicate this humble work to the sake of Allah Almighty, seeking His acceptance, aspiring to His pleasure, and in response to a deep conviction I carry: that knowledge leaves an imprint, sincere intentions carry weight, and each devoted step echoes beyond its time.

I hope that Allah places acceptance for it in the heavens and the earth.

I pray that this effort stands as a small stone laid in the path of service and benefit to the Ummah an offering in support of its mission and the raising of its banners of goodness, under a faith that taught us the power of a kind word, and that knowledge is a lasting inheritance.

I dedicate it to my homeland its soil, its history, and its hope.

To my beloved parents, whose presence has been a source of strength, prayer, and unwavering support at every step.

To my brothers and sisters, who have shared the meaning long before the journey began, and to all my family, whose love carried me and whose patience sustained me, both near and far, seen and unseen.

I also dedicate this work to the students who come after me, the seekers of knowledge who will carry the torch down ever-evolving paths perhaps different from ours, but requiring the same sincerity, faith, and determination.

To whoever opens these pages in search of understanding or a new step forward, I hope you find something here to support and inspire you, even in the smallest way.

This work is the fruit of a journey woven with learning and reflection, perseverance and trust, patience and quiet devotion. It is a path I walked with the hope that its impact may outlive its author.

To all those who had a hand, a prayer, or a silent kindness along the way whether near or distant and to all Muslims, men and women, living or departed, I pray that Allah grants them a share of the reward, and that He makes this work among that which is beneficial, remembered, and weighty in the scales.

This is but a beginning of what I hope will be a lasting path in the service of knowledge and humanity

.

Acknowledgments

By the grace and guidance of Allah, this work has been completed. It is through His support that strength and perseverance are sustained.

Every word of thanks written here is a modest attempt to express the deep gratitude I hold for all those who supported me throughout this journey.

To my supervisor, who offered more than academic guidance thank you for your time, attention, and thoughtful direction, which were essential to the success of this research.

To the professors who helped build bridges of knowledge and insight your impact has gone far beyond lectures and textbooks, and I deeply value your contributions.

I cannot proceed without acknowledging my family, who have been a constant source of strength and calm.

To my parents, who instilled patience and persistence in me, and to my siblings and loved ones, who quietly supported me through the difficult moments you have been my true foundation.

A sincere thank you as well to my friends and colleagues, whose presence transformed challenges into opportunities and whose encouragement made the path easier.

To everyone who left a mark, no matter how small thank you.

I pray that this work may become a shared benefit and a lasting good for all.

Contents

List of figures

List of Tables

General Introduction

General introduction

The growing concerns about climate change, pollution, and the depletion of natural resources have pushed the world to reconsider its heavy dependence on fossil fuels [1]. For decades, fossil fuels like coal, oil, and natural gas have been the backbone of global energy production. However, their continued use has caused serious environmental issues, especially the emission of greenhouse gases that contribute to global warming.

As the search for cleaner and more sustainable energy sources intensifies, hydrogen has gained significant attention. It is a clean fuel that produces only water when used and has a high energy content, making it suitable for many modern applications [2]. Still, one of the biggest challenges with hydrogen is how to store and transport it safely and efficiently, which limits its large-scale use [3].

To tackle this challenge, researches have been exploring solid-state hydrogen storage, especially using materials known as metal hydrides. These compounds can store hydrogen within their structure and release it when needed, which could be a safer and more practical solution compared to storing hydrogen in gas or liquid form [4].

One material that has drawn interest in this field is lutetium hydride LuH_2. Lutetium is one of the rare-earth elements, a group of metals that, despite the name, are not actually rare in the Earth's crust, The name" rare-earth"comes from the fact that they are not usually found in pure form, but rather as oxides spread throughout the earth [5]. These elements have unique properties that make them valuable in many advanced technologies, including hydrogen storage.

By using a method called Density Functional Theory (DFT), researchers can study how LuH_2 behaves on an atomic level-how stable it is, how it stores hydrogen and how it might perform in real-world applications [6]. This type of research helps build the knowledge needed to make hydrogen a reliable and widely used energy source in the future, contributing to a more sustainable and less fossil-fuel-dependent world.

References

[1] Balta-Ozkan, N., Yildirim, J., & Connor, P. M. (2015). Energy transitions: policy and planning. Energy Policy, 83, 396–403.

[2] Crabtree, G. W., Dresselhaus, M. S., & Buchanan, M. V. (2004). The hydrogen economy. Physics Today, 57(12), 39–44. 3. Züttel, A. (2003). Materials for hydrogen storage. Materials Today, 6(9), 24–33. (03)00922-2

[4] Schlapbach, L., & Züttel, A. (2001). Hydrogen-storage materials for mobile applications. Nature, 414(6861), 353–358. 5. Gschneidner Jr, K. A., & Eyring, L. (2000). Handbook on the Physics and Chemistry of Rare Earths (Vol. 30). Elsevier.

[6] Jones, R. O., & Gunnarsson, O. (1989). The density functional formalism, its applications and prospects. Reviews of Modern Physics, 61(3), 689.

Chapter 1:

General Overview of Hydrogen and Rare Earth Hydrides

1.1. Introduction

As the world faces growing environmental problems caused by fossil fuels, hydrogen is becoming a cleaner and more sustainable energy option [1]. One of the biggest challenges, though, is how to store it efficiently [2]. That's where materials like lutetium hydride (LuH_2) [3].

1.2. A brief history of hydrogen

Henry Cavendish discovered that hydrogen was a flammable gas in the 18th century, which led to its first identification as a separate element. After learning that it produces water when burned, Antoine Lavoisier later gave it the name "hydrogen," which translates to "water-former" in Greek [4, 5]. Since then, hydrogen has been essential to technological advancements and scientific discoveries, particularly in the fields of energy and space applications [6].

1.3. Hydrogen production methods

There are several methods for hydrogen production [7, 8], including:

1.3.1. Thermochemical Processes

Certain thermal processes release hydrogen from their molecular structure by using the energy found in different resources, such as coal, biomass, or natural gas. In other processes, heat and closed-chemical cycles combine to create hydrogen from feedstocks like water. For instance, hydrogen derived from coal gasification is typically categorized as black or brown hydrogen due to high carbon emissions. Conversely, when natural gas is used with capture technologies, the product is known as blue hydrogen, offering a lower-carbon alternative.

1.3.2. Electrolytic Processes

Electrolyzers separate water into hydrogen and oxygen using electricity. Systems that can effectively use intermittent renewable power are being developed, and this technology is well-developed and commercially available. If renewable energy sources power the electrolyzer, the resulting hydrogen is termed green hydrogen, reflecting its minimal carbon footprint. If electricity from mixed or non-renewable sources is used, the hydrogen is often referred to as yellow hydrogen.

1.3.3. Direct solar water splitting Processes

Photolytic processes, also known as direct solar water splitting, use light energy to split water into hydrogen and oxygen. Although research on these processes is still in its early phases, they have the potential to produce hydrogen in the long run with minimal negative effects on the environment, these methods aim to produce green hydrogen in the future

1.3.4. Biological Processes

Through biological processes utilizing sunlight or organic matter, microorganisms like bacteria and microalgae are able to produce hydrogen. Hydrogen produced via such biological pathways is generally considered green due to the low-carbon nature of the source materials. Although these methods are still in the research and development stage, they hold promise for future sustainable hydrogen production.

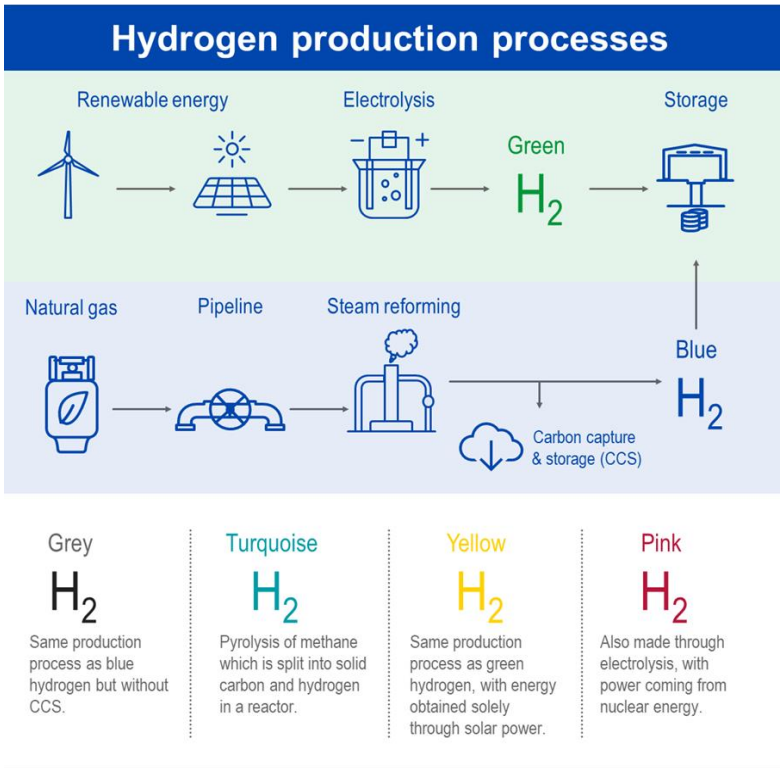

Figure (1-1): Hydrogen production processes.

1.4. Hydrogen storage

1.4.1. Compressed Hydrogen Storage

Hydrogen is stored in its gaseous form within cylinders or tanks at elevated pressures, typically ranging from 350 to 700 bar. This method is widely used in various transportation applications, particularly in vehicles powered by fuel cells [9].

1.4.2. Liquid Hydrogen Storage

Hydrogen is converted into a liquid by cooling it to 253℃ and is then stored in highly insulated cryogenic tanks. This approach offers a higher energy density but requires substantial energy for the liquefaction process, as well as advanced thermal insulation to maintain the low temperatures [10].

1.4.3. Chemical Hydrogen Storage

In this method, hydrogen is stored within chemical compounds like ammonia (NH_3) or formic acid, which release hydrogen when exposed to heat or catalysts. This storage technique is particularly favored for its safety and ease of transport [11]

1.4.4. Solid-State Storage

Solid-state storage refers to a group of methods in which hydrogen is stored within or on the surface of solid materials. This category includes three main approaches: adsorption, reversible absorption, and storage via metal hydrides. These methods are known for their high safety levels and potential for long-term hydrogen storage [12].

1.4.4.1. Adsorption

This method relies on the physical binding of hydrogen molecules to the surface of materials with exceptionally high surface areas, such as activated carbon or metal-organic frameworks (MOFs), through van der Waals forces. Since no chemical bonds are formed, adsorption is a reversible and fast-response storage method [13].

1.4.4.2. Reversible Absorption

In reversible absorption, hydrogen is absorbed into the crystal lattice of solid materials, forming compounds known as metal hydrides. Upon heating, the hydrogen is released, making this a fully reversible process. This approach offers high storage density and is well-suited for applications requiring safety and thermal stability.

- **Metal Hydrides**

Metal hydrides store hydrogen by absorbing it into the metal's crystal lattice, allowing safe, compact storage at moderate pressures and temperatures. This method offers higher volumetric density compared to gaseous or liquid hydrogen. Metal hydrides are ideal for stationary and mobile applications due to their safety and efficiency [14].

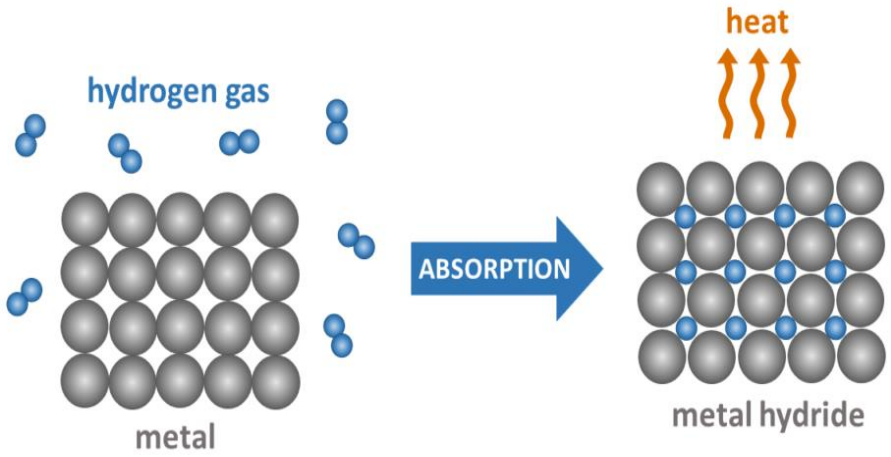

Figure (1-2): Mechanism of metal hydride formation via hydrogen absorption [15].

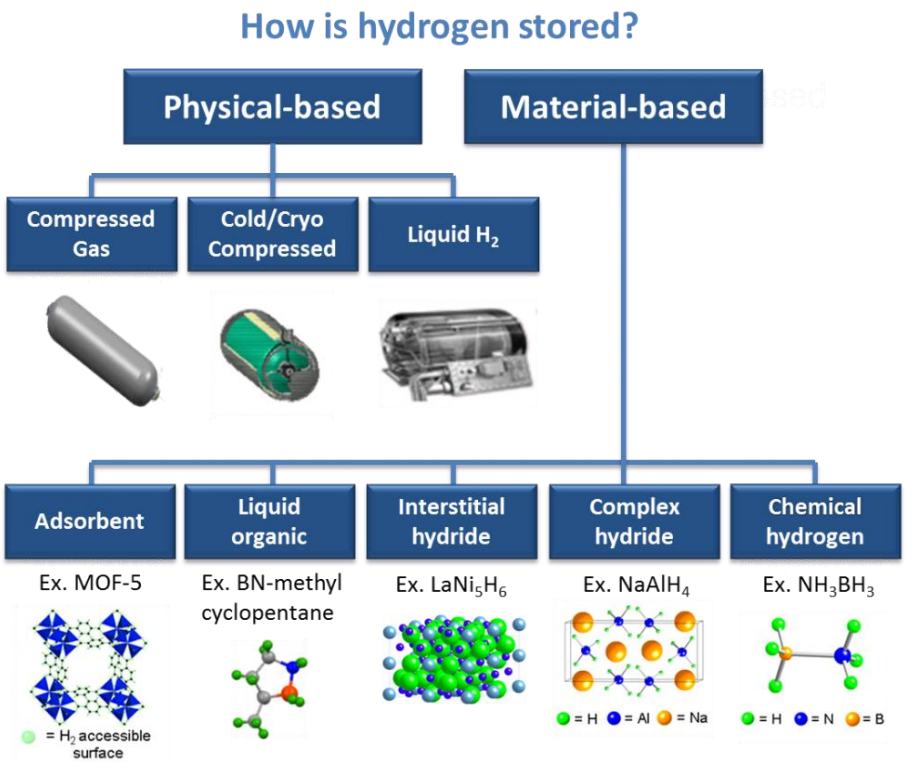

Figure (1-3): Various hydrogen storage methods [16].

1.5. Hydrogen Delivery

Hydrogen delivery is a key component in developing a clean energy economy. It requires transporting hydrogen from production sites to end-use points, such as refueling stations or industrial plants. This requires an integrated and efficient infrastructure, which includes facilities such as pipelines, liquefaction plants, storage systems, compression units, and specialized transport vehicles [17].

1.5.1. Methods of hydrogen transport

1.5.1.2. Pipeline Transport

This is one of the most efficient methods for transporting large quantities of compressed hydrogen over long distances. However, it requires significant investment in infrastructure and the use of materials that can withstand hydrogen embrittlement.

1.5.1.3. Truck Transport

Trucks are used to transport hydrogen either in gaseous form (via compressed gas trucks) or liquid form (via refrigerated tankers). This method is flexible for delivering hydrogen to locations not connected to pipeline networks but is more expensive in terms of operational costs.

1.5.1.4. Rail and Ship Transport

This method is suited for transporting large quantities of hydrogen or hydrogen carriers, such as ammonia, over long distances, especially for international transport. However, it requires specialized equipment and careful handling of hazardous materials.

1.5.2. Alternative Hydrogen Carriers

To overcome storage and transportation challenges, hydrogen is sometimes transported as a chemical carrier, such as:

1.5.2.1. Ammonia (NH_3)

Easily transported and later converted back to hydrogen at the point of use.

1.5.2.2. Liquid Organic Hydrogen Carriers (LOHC)

Allow hydrogen to be stored and transported under moderate pressure and temperature, reducing risks and enhancing safety.

1.5.3. Technical and Economic Challenges

1.5.3.1. Hydrogen Embrittlement

Hydrogen can interact with certain metals, weakening their mechanical properties, which presents a challenge in designing hydrogen transport systems.

1.5.3.2. High Costs

The infrastructure for hydrogen delivery requires significant investments, which is a barrier to widespread deployment.

1.5.3.3. Lack of Current Infrastructure

Many regions still lack integrated hydrogen transport and distribution networks, limiting the efficiency of supply chains.

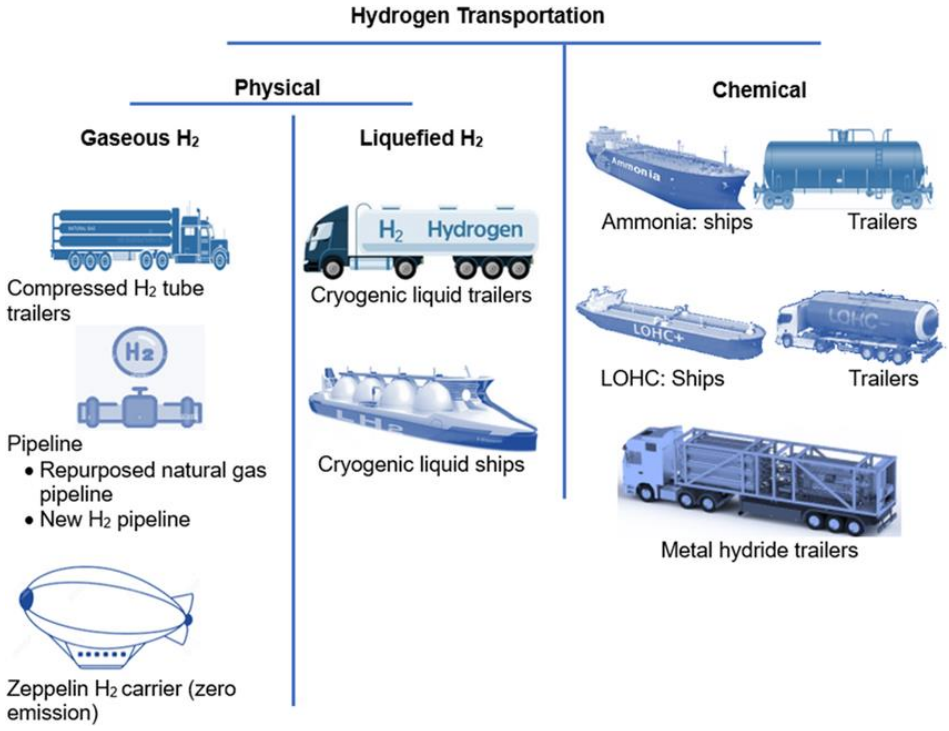

Figure (1-4): Different hydrogen transportation methods [18].

1.6. The hydrides

Hydrides are chemical compounds in which hydrogen is bonded to another element, often exhibiting nucleophilic, reducing, or basic properties. In many of these compounds, hydrogen acts as a hydride ion, and its behavior varies depending on the nature of the element it bonds with [19].

1.6.1. Types of hydrides

1.6.1.1. Covalent Hydrides

These are formed when hydrogen bonds covalently with non-metallic elements. They often exist as discrete molecules and include compounds such as water (H_2O), ammonia (NH_3), and methane (CH_4). Some covalent hydrides, like borohydrides BH_4, feature multi-center bonding [20].

1.6.1.2. Interstitial Metallic Hydrides

In these hydrides, hydrogen atoms occupy interstitial spaces within the crystal lattice of transition and rare earth metals. They do not form classical covalent bonds but rather interact with the metallic electron cloud, resulting in metallic conductivity. They are widely used in hydrogen storage applications.

Metal hydrides are among the most important materials used for hydrogen storage due to their ability to absorb and release hydrogen under suitable thermal and pressure conditions. Many of these hydrides are classified based on the stoichiometric ratio between the metal (A) and the other element or hydrogen (B). Common types include AB, AB_2, AB_3, AB_5, and A_2B. These hydrides differ in structural properties and thermochemical behavior, making each type suitable for specific applications in clean energy technologies. [21].

1.6.1.2.1. AB-Type Hydrides (1:1 Ratio)

AB-type hydrides represent the simplest structural form, where a metal reacts with hydrogen in a 1:1 ratio. A well-known example is the FeTi compound, which features good thermal stability and reversible hydrogen absorption and desorption at moderate temperatures. This makes it a promising candidate for energy storage applications. Such hydrides play a key role in increasing efficiency in renewable energy systems [22].

1.6.1.2.2. AB_2-Type Hydrides (1:2 Ratio)

AB_2-type hydrides, such as $ZrMn_2$ and ZrV_2, are favored for hydrogen storage due to their high reactivity and easy activation. These compounds rapidly absorb hydrogen without requiring additional catalysts, making them suitable for high-performance industrial applications. They also offer a good balance between storage capacity and reaction speed [21].

1.6.1.2.3. AB_3-Type Hydrides (1:3 Ratio)

Although less common, AB_3-type hydrides like LaH_3 are notable for their high hydrogen density. These hydrides often involve rare earth elements and possess complex crystal structures that allow for efficient hydrogen storage within the lattice interstices. Their stability under moderate conditions makes them attractive for long-term storage in clean energy systems [23].

1.6.1.2.4. AB_5-Type Hydrides (1:5 Ratio)

Among the most well-known hydrides is the AB_5 type, particularly $LaNi_5$, which is widely used in nickel-metal hydride (NiMH) rechargeable batteries. These materials exhibit high efficiency and rapid hydrogen kinetics, with stable cyclic behavior, making them ideal for portable energy storage and electric vehicles [24].

1.6.1.2.5. A_2B-Type Hydrides (2:1 Ratio)

Hydrides of the A_2B type, such as Mg_2Ni, are lightweight and effective in terms of hydrogen storage density. These compounds demonstrate good reversibility and reaction kinetics, along with thermal stability under moderate operating conditions. They are especially suited for applications requiring high storage density and low mass, such as aerospace systems and portable fuel cells [21].

1.6.1.3. Ionic (Salt-like) Hydrides

These are typically formed by the reaction of hydrogen with highly electropositive metals such as alkali and alkaline earth metals. The bonding is primarily ionic, involving the formation of hydride ions (H^-). These hydrides react vigorously with water and are strong bases [25].

1.7. Rare earth elements

Rare earth elements (REEs) are a group of 17 chemically similar elements, comprising the 15 lanthanides in the periodic table, along with scandium and yttrium. Despite their name, these elements are relatively abundant in the Earth's crust, but their dispersion makes them rarely found in concentrated and economically viable deposits. Their extraction and separation are technically complex and environmentally challenging due to their similar ionic radii and chemical behavior. REEs exhibit remarkable magnetic, electrical, and luminescent properties, which make them indispensable in a wide range of advanced technologies. These include high-performance permanent magnets (used in wind turbines and electric vehicles), rechargeable batteries, phosphors in lighting and displays, and catalysts in various industrial processes.

The history of REEs dates back to 1794, when Finnish chemist Johan Gadolin discovered yttrium after analyzing the black mineral gadolinite, which had been found earlier in 1787 near the village of Ytterby in Sweden. This village later lent its name to several rare earth

elements, such as terbium, erbium, and ytterbium. Since then, rare earth chemistry has developed into a critical field for both academic research and industrial innovation [26-29].

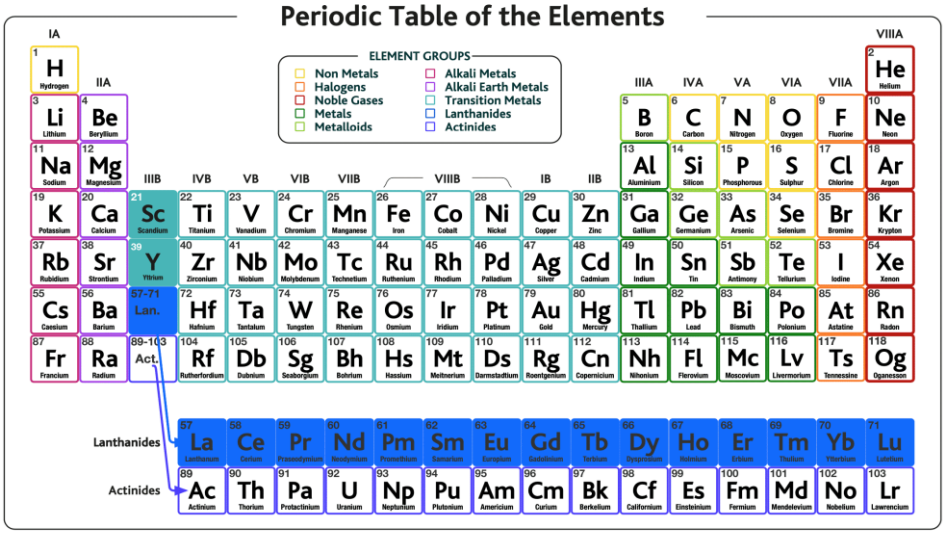

Figure (1-5): periodic table of chemical elements [30].

1.8. Rare earth hydrides

Rare-earth hydrides are formed when rare-earth elements react with hydrogen, initially producing. Hydrogen is stored in rare-earth elements in the form of atoms within their crystal lattice, occupying unfilled interstitial sites, either tetrahedral or octahedral

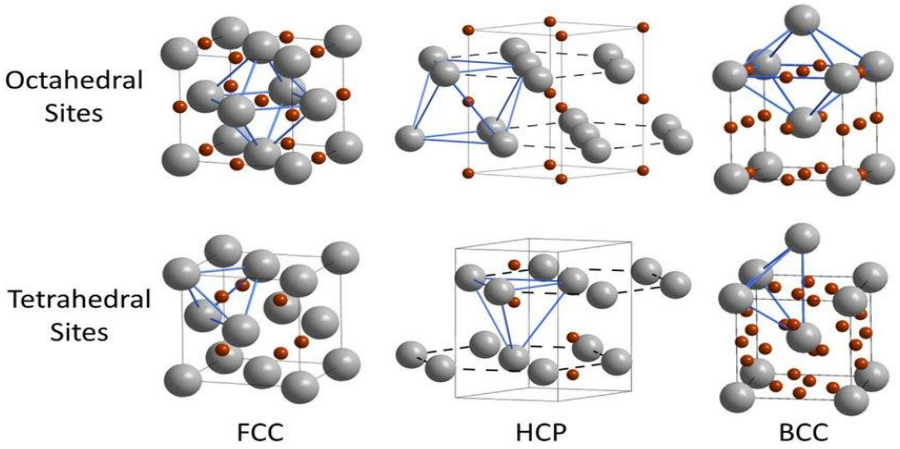

Figure (1-6): Interstitial sites in the crystal structure [31].

RH_2 compounds. Under increased hydrogen pressure, most trivalent rare-earth elements also form RH_3 compounds. Both phases are nonstoichiometric, meaning their hydrogen content can vary. The RH_2 phase typically crystallizes in the CaF_2 (fluorite) structure, while divalent europium (Eu) and ytterbium (Yb) form dihydrides with an orthorhombic structure. The RH_3 phase has a fluorite-like structure for light rare earths and a hexagonal structure for the heavier elements [32].

These hydrides are highly air-sensitive and must be handled in inert environments. The electrical resistivity of RH_2 is significantly lower than that of the pure metal, but it increases with hydrogen content and approaches semiconducting behavior in RH_3. For example, LaH_3 is diamagnetic and exhibits semiconducting properties. Many RH_2 compounds are ferromagnetic or antiferromagnetic, and EuH_2 is ferromagnetic at low temperatures (-248.15°C) [33].

Additionally, switchable mirror systems based on YH_x and LaH_x have been developed, where the optical properties shift from reflective to transparent as hydrogen concentration increases toward $x \approx 3$. This effect has since been extended to other rare-earth elements and alloys involving magnesium and various transition metals [34].

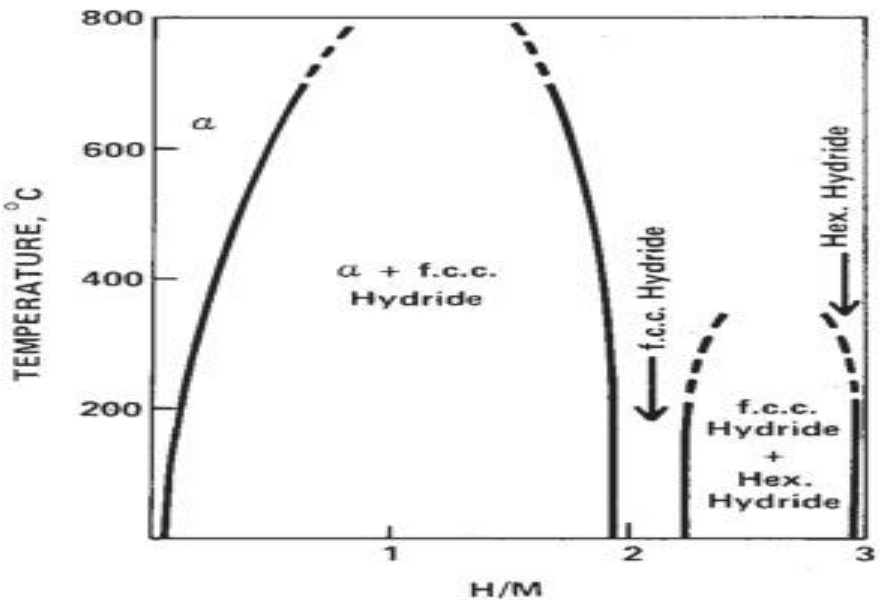

Figure (1-7): Phase diagram of trivalent rare earth elements [35].

1.9. Lutetium

Lutetium (Lu), the final element in the lanthanide series (atomic number 71), is distinguished by its fully filled 4f orbital ($4f^{14}$), which contributes to its electronic stability. It is one of the rarest and most dense rare-earth elements, discovered in 1907. Lutetium usually appears in the +3 oxidation state and has a high melting point, significant hardness, and metallic behavior.

Figure (1-8): Crystalline sample of lutetium metal [36].

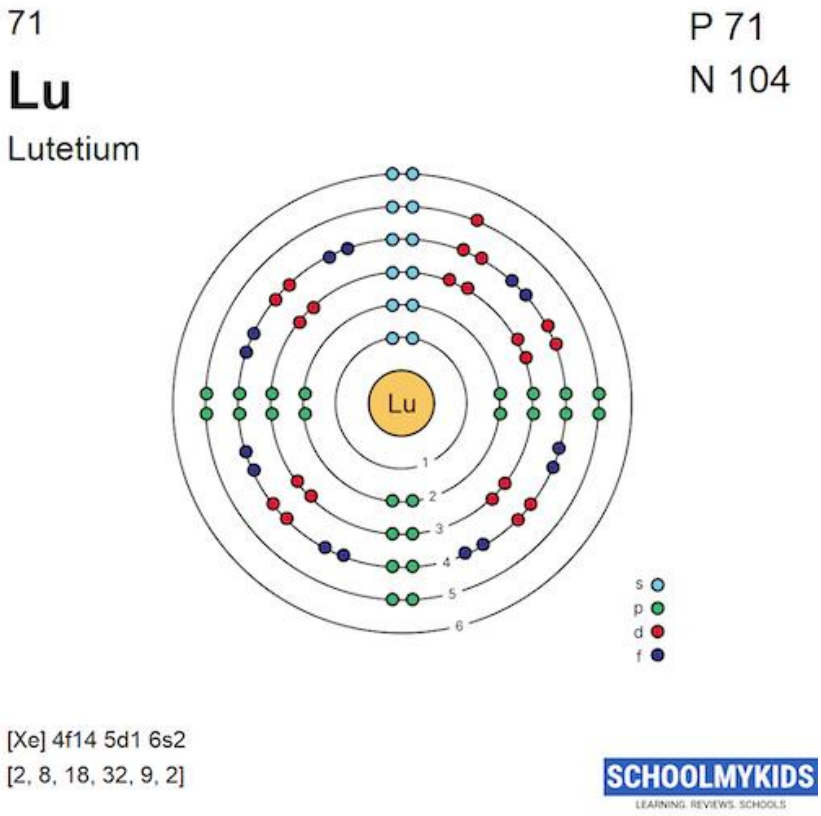

Figure (1-9): Electronic configuration of lutetium metal [37].

Although its rarity limits large-scale industrial use, it plays an essential role in specialized applications, such as petroleum refining catalysts and phosphor materials. In the medical field, the radioactive isotope ^177Lu is widely used in targeted radiotherapy for cancers, including neuroendocrine and prostate tumors.

Lutetium shows metallic conductivity with resistivity increasing nearly linearly with temperature. It remains paramagnetic across most temperatures but may exhibit weak magnetic transitions at low temperatures due to defects or impurities [38].

1.10. Lutetium Dihydride:

Lutetium dihydride (LuH_2) is an inorganic compound composed of the rare-earth metal lutetium and hydrogen. It has the chemical formula LuH_2 and a molecular weight of approximately 193.97 g/mol. The compound appears as a gray metallic solid, is insoluble in water, and crystallizes in a stable fluorite-type cubic structure under standard conditions. According to IUPAC nomenclature, its systematic name is dihydrolutetium [21].

LuH_2 is typically synthesized by directly reacting metallic lutetium with hydrogen gas at elevated temperatures (300–500 °C), following the reaction:

$$Lu + H_2 \rightarrow LuH_2 \quad (1\text{-}1)$$

This reaction requires controlled conditions to ensure the formation of the dihydride phase and to avoid the emergence of higher hydrides such as LuH_3 [21]. The resulting material exhibits thermal stability and retains a robust metal–hydrogen bonding framework.

The compound is of particular interest in hydrogen storage applications due to its ability to reversibly absorb and release hydrogen [38]. It also shows electrical conductivity with temperature-independent resistivity, a behavior typical of metallic hydrides with strong electron scattering [39]. Magnetically, LuH_2 remains paramagnetic over a wide temperature range and lacks clear evidence of long-range magnetic ordering.

Recent theoretical and computational studies have explored its vibrational and electronic properties, especially under high-pressure conditions or in doped configurations

(e.g., nitrogen doping). These investigations highlight LuH_2 as a promising material for advanced applications in energy storage and quantum materials research, including the exploration of novel superconducting states [40-42].

Summary

In this chapter, we presented the main methods of hydrogen production and its various storage forms, with a focus on rare earth elements due to their ability to store hydrogen in interstitial crystal sites under suitable pressure and temperature conditions. As a prelude to our study, we discussed the hydrides of these elements—particularly lutetium hydride (LuH_2)—which exhibits promising physical properties for hydrogen storage. This chapter provides a theoretical foundation for analyzing the structural, electronic, and optical properties of this compound using Density Functional Theory (DFT).

References

[1] Turner, J. A. (2004). Sustainable hydrogen production. *Science*, *305*(5686), 972-974.

[2] Schlapbach, L., & Züttel, A. (2001). Hydrogen-storage materials for mobile applications. Nature, 414(6861), 353–358.

[3] Grochala, W., & Edwards, P. P. (2004). Thermal decomposition of the non-interstitial hydrides for the storage and production of hydrogen. Chemical Reviews, 104(3), 1283–1315.

[4] Ogunsola, O. I., & Ogunsola, O. M. (2024). *Hydrogen Technologies: Production, Transportation, Storage, and Utilization*. CRC Press.

[5] Weeks, M. E. (1933). The discovery of the elements. XIX. The radioactive elements. *Journal of Chemical Education*, *10*(2), 79.

[6] Gunathilake, C., Soliman, I., Panthi, D., Tandler, P., Fatani, O., Ghulamullah, N. A., ... & Jaroniec, M. (2024). A comprehensive review on hydrogen production, storage, and applications. *Chemical Society Reviews*, *53*(22), 10900-10969.

[7] Elgowainy, A., Mintz, M., Lee, U., Stephens, T., Sun, P., Reddi, K., ... & Boardman, R. (2020). *Assessment of potential future demands for hydrogen in the United States* (No. ANL-20/35). Argonne National Lab.(ANL), Argonne, IL (United States).

[8] Bruce, S., Temminghoff, M., Hayward, J., Schmidt, E., Munnings, C., Palfreyman, D., & Hartley, P. (2018). National hydrogen roadmap. *Australia: CSIRO*, *92*.

[9] Erdoğan, A., Geçici, E., & Güler, M. G. (2023). Design of a future hydrogen supply chain: A multi-objective model for Turkey. *International Journal of Hydrogen Energy*, *48*(31), 11775-11789.

[10] Satyapal, S., Petrovic, J., Read, C., Thomas, G., & Ordaz, G. (2007). The US Department of Energy's National Hydrogen Storage Project: Progress towards meeting hydrogen-powered vehicle requirements. *Catalysis today*, *120*(3-4), 246-256.

[11] Kumar, R., & Singh, R. (2022). Hydrogen storage methods: Review and current status. Renewable and Sustainable Energy Reviews, 163, 112538.

[12] Sakintuna, B., Lamari-Darkrim, F., & Hirscher, M. (2007). Metal hydride materials for solid hydrogen storage: a review. *International journal of hydrogen energy*, *32*(9), 1121-1140.

[13] Shi, W., Jin, X., Zhang, C., Zhang, X., Liu, X., Gao, Y., ... & Li, A. (2024). Recent advancement in metal-organic frameworks for hydrogen storage: Mechanisms, influencing factors and enhancement strategies. *International Journal of Hydrogen Energy*, *83*, 432-449.

[14] Kojima, Y., Kawai, Y., Towata, S. I., Matsunaga, T., Shinozawa, T., & Kimbara, M. (2006). Development of metal hydride with high dissociation pressure. *Journal of alloys and compounds*, *419*(1-2), 256-261.

[15] Lototskyy, M., & Linkov, V. (2022). Thermally driven hydrogen compression using metal hydrides. *International Journal of Energy Research*, *46*(15), 22049-22069.

[16] Law, K., Rosenfeld, J., Han, V., Chan, M., Chiang, H., & Leonard, J. (2013). *US Department of energy hydrogen storage cost analysis* (No. DOE/GO14283). TIAX LLC.

[17] Elgowainy, A., Mintz, M., Lee, U., Stephens, T., Sun, P., Reddi, K., ... & Boardman, R. (2020). *Assessment of potential future demands for hydrogen in the United States* (No. ANL-20/35). Argonne National Lab.(ANL), Argonne, IL (United States).

[18] Omid, M. A., Şahin, M. E., & Cora, Ö. N. (2024). Challenges and future perspectives on production, storage technologies, and transportation of hydrogen: a review. *Energy Technology*, *12*(4), 2300997.

[19] Metil, D. S., Sonawane, S. P., Pachore, S. S., Mohammad, A., Dahanukar, V. H., McCormack, P. J., ... & Bandichhor, R. (2018). Synthesis and optimization of canagliflozin by employing quality by design (QbD) principles. *Organic Process Research & Development*, *22*(1), 27-39.

[20] Greenwood, N. N., & Earnshaw, A. (1997). *Chemistry of the elements 2nd Edition*. Butterworth-Heinemann.

[21] Schlapbach, L., & Züttel, A. (2001). Hydrogen-storage materials for mobile applications. *nature*, *414*(6861), 353-358.

[22] Humphries, T. D., Buckley, C. E., Paskevicius, M., & Jensen, T. R. (2023). State-of-the-Art and Progress in Metal-Hydrogen Systems. *Inorganics*, *11*(12), 476.

[23] Fukai, Y. (2006). *The metal-hydrogen system: basic bulk properties* (Vol. 21). Springer Science & Business Media.

[24] Bogdanović, B., & Schwickardi, M. (1997). Ti-doped alkali metal aluminium hydrides as potential novel reversible hydrogen storage materials. *Journal of alloys and compounds*, *253*, 1-9.
[25] Wiberg, E., & Wiberg, N. (2001). *Inorganic chemistry*. Academic press.

[26] Gschneidner, K. A., Bunzli, J. C. G., & Pecharsky, V. K. (2004). *Handbook on the physics and chemistry of rare earths* (Vol. 34). Elsevier. [29] Gschneidner, K. A., & Eyring, L. (2000). Rare Earths: Science, Technology and Applications. Royal Society of Chemistry.

[27] Gupta, C. K., & Krishnamurthy, N. (1992). Extractive metallurgy of rare earths. *International materials reviews*, *37*(1), 197-248.

[28] Haxel, G. (2002). *Rare earth elements: critical resources for high technology* (Vol. 87, No. 2). US Department of the Interior, US Geological Survey.

[29] Ilankoon, I. M. S. K., Dushyantha, N. P., Mancheri, N., Edirisinghe, P. M., Neethling, S. J., Ratnayake, N. P., ... & Batapola, N. M. (2022). Constraints to rare earth elements supply

diversification: Evidence from an industry survey. *Journal of Cleaner Production*, *331*, 129932. [30] Chao, B., & Klebanoff, L. (2012). Hydrogen storage in interstitial metal hydrides. *Hydrogen storage technology, materials and applications*, 109..

[31] Eyring, L., Gschneidner, K. A., & Lander, G. H. (Eds.). (2002). *Handbook on the physics and chemistry of rare earths* (Vol. 32). Elsevier.

[32] Gupta, C. K., & Krishnamurthy, N. (1992). Extractive metallurgy of rare earths. *International materials reviews*, *37*(1), 197-248.

[33] Huiberts, J. N., Griessen, R., Rector, J. H., Wijngaarden, R. J., Dekker, J. P., De Groot, D. G., & Koeman, N. J. (1996). Yttrium and lanthanum hydride films with switchable optical properties. *Nature*, *380*(6571), 231-234.

[34] Martins, F. P., Almaraz, S. D. L., Junior, A. B. B., Azzaro-Pantel, C., & Parikh, P. (2024). Hydrogen and the sustainable development goals: synergies and trade-offs. *Renewable and Sustainable Energy Reviews*, *204*, 114796.

[35] Getty Images. (n.d.). Lutetium – A piece of lutetium metal [Photograph]. Retrieved May 26, 2025.

[36] Hassan, F. Lanthanide and Actinide Chemistry.

[37] Ferrucci, B., Ottaviano, G., Rizzo, A., & Ubaldini, A. (2022). Future development of global molybdenum-99 production and saving of atmospheric radioxenon emissions by using nuclear fusion-based approaches. *Journal of Environmental Radioactivity*, *255*, 107049.

[38] Eyring, L., Gschneidner, K. A., & Lander, G. H. (Eds.). (2002). *Handbook on the physics and chemistry of rare earths* (Vol. 32). Elsevier.

[39] Hao, X., Wei, X., Liu, H., Song, X., Sun, R., Gao, G., & Tian, Y. (2023). First-principles calculations on structural stability and electronic properties of nitrogen-doped lutetium hydrides under pressure. *Physical Review Research*, *5*(4), 043238.

[40] Zhang, S., Bi, J., Zhang, R., Li, P., Qi, F., Wei, Z., & Cao, Y. (2023). Electronic and magnetic properties of Lu and LuH2. *AIP Advances*, *13*(6).

[41] Dangić, Đ., Garcia-Goiricelaya, P., Fang, Y. W., Ibañez-Azpiroz, J., & Errea, I. (2023). Ab initio study of the structural, vibrational, and optical properties of potential parent structures of nitrogen-doped lutetium hydride. *Physical Review B*, *108*(6), 064517.

Chapter 2:

Density Functional Theory (DFT) and the WIEN2k Computational

2.1. Introduction

Density Functional Theory (DFT) is a computational method used in solid-state physics and quantum chemistry to study the electronic properties of materials. It is based on the idea that the electron density determines all physical properties of a system, which simplifies calculations compared to using the many-body wave function.

The theory was established by Hohenberg and Kohn (1964) and made practically applicable by Kohn and Sham (1965) [1, 2].

In this chapter, we briefly address the Schrödinger equation, which is analytically unsolvable for many-electron systems, necessitating the use of computational approximations such as Density Functional Theory (DFT). We also present the main computational methods integrated into simulation software, followed by a general overview of the WIEN2k program, which is based on DFT, along with its key features and capabilities.

2.2. Schrödinger equation

The Schrödinger equation is a fundamental cornerstone of quantum mechanics. It is used to describe the quantum state of many-particle systems, such as electrons and nuclei in atoms, molecules, and solids. The time-independent form of the equation is written as:

$$H\psi = E\psi \tag{2-1}$$

Where:

ψ: Wave function of the system.

E: Total energy of the system.

H: Hamiltonian of the system.

$$H = T_e + T_N + V_{ee} + V_{eN} + V_{NN} \tag{2-2}$$

T_e: Kinetic energy of electrons.

$$T_e = \sum_i \frac{p_i^2}{2m_i} = \sum_i -\frac{\hbar^2}{2m_i}(\nabla_i^2) \tag{2-3}$$

$$T_N = \sum_\alpha \frac{p_\alpha^2}{2M_\alpha} = \sum -\frac{\hbar^2}{2M}(\nabla_\alpha^2) \quad (2\text{-}4)$$

m: Mass of electrons.

M: Mass of nuclei.

(∇_i^2): Laplacian operator.

$$(\nabla_i^2) = \frac{\partial^2}{\partial x^2} + \frac{\partial^2}{\partial y^2} + \frac{\partial^2}{\partial z^2} \quad (2\text{-}5)$$

V_{ee}: Electron-electron interaction energy.

$$V_{ee} = \sum_{i,j\neq i} \frac{1}{4\pi\varepsilon_0}\frac{1}{2}\left[\frac{e^2}{|\vec{r_i}-\vec{r_j}|}\right] \quad (2\text{-}6)$$

$|\vec{r_i} - \vec{r_j}|$: Distance between electrons i and j

V_{eN}: Electron-nucleus interaction energy.

$$V_{eN} = \frac{1}{4\pi\varepsilon_0}\sum_{i,\alpha} -\frac{e^2 z_\alpha}{|\vec{r_i}-\overrightarrow{R_\alpha}|} \quad (2\text{-}7)$$

$|\vec{r_i} - \overrightarrow{R_\alpha}|$: Distance between nucleus α and electron i.

V_{NN}: Nucleus-nucleus interaction energy.

$$V_{NN} = \frac{1}{4\pi\varepsilon_0}\frac{1}{2}\sum_{\alpha,\beta\neq\alpha} \frac{e^2 z_\alpha z_\beta}{|\overrightarrow{R_\alpha}-\overrightarrow{R_\beta}|} \quad (2\text{-}8)$$

$|\overrightarrow{R_\alpha} - \overrightarrow{R_\beta}|$: Distance between nucleus α and nucleus β.

In the stationary case, the Schrödinger equation becomes time-independent and is written as follows:

$$H\psi(r,R) = E\psi(r,R) \quad (2\text{-}9)$$

ψ: A wave function that depends on all the coordinates of the particles.

E: The eigenvalue corresponding to the wave function.

The Schrödinger equation cannot be solved exactly because this description involves a large number of degrees of freedom. Therefore, several approximations have been introduced to simplify and solve it [3].

2.3. Born-Oppenhaimer approximation

The Born–Oppenheimer approximation simplifies the quantum mechanical treatment of molecules by assuming that the nuclei remain stationary during the motion of electrons due to their much larger mass. This separation allows solving the electronic Schrödinger equation independently of nuclear motion, which significantly reduces computational complexity.

The electronic Hamiltonian is written as:

$$H_e = T_e + V_{ee} + V_{eN} \tag{2-10}$$

And the time-independent electronic Schrödinger equation becomes:

$$H_e\psi_e = E_e\psi_e \tag{2-11}$$

This approximation forms the basis of most electronic structure calculations, including Density Functional Theory (DFT). However, solving the resulting equations remains complex, which necessitated the development of further approximations such as the Hartree–Fock method [3. 4].

2.4. Hartree–Fock Approximation

The Hartree–Fock approximation further simplifies the many-electron problem by modeling each electron as moving independently in an average electrostatic field created by the other electrons and nuclei. This approach assumes that the total wave function is a product of single-electron wave functions [3, 4].

The total Hamiltonian of the system is:

$$H = \sum_{i=1}^{N} H_i \tag{2-12}$$

The single-electron Hamiltonian is expressed as:

$$H_i = -\frac{-\hbar^2}{2m}\Delta_i + U_i(r_i) + V_i(r_i) \tag{2-13}$$

$U_i(r_i)$: The potential energy of electron i in the field of nuclei k.

$$U_i(r_i) = -\sum_k \frac{z_k e^2}{4\pi\varepsilon_0|\overrightarrow{R_k}-\overrightarrow{r_i}|} \quad (2\text{-}14)$$

$\overrightarrow{R_k}$: The position of nucleus k.

$V_i(r_i)$: The Hartree effective potential.

$$V_i(r_i) = -\frac{1}{2}\sum_i \frac{e^2}{4\pi\varepsilon_0|\overrightarrow{r_i}-\overrightarrow{r_j}|} \quad (2\text{-}15)$$

The total wave function is approximated as:

$$\psi_{(r_1,r_2,\ldots\ldots)} = \prod_{i=1}^{N} \psi_i(r_i) \quad (2\text{-}16)$$

And the total energy of the system is:

$$E = \sum E_i \quad (2\text{-}17)$$

Consequently, the Schrödinger equation takes the following form:

$$\left[-\frac{1}{2}\frac{\hbar^2}{m}\Delta_i + U_i(r_i) + V_i(r_i)\right]\psi_i(r) = \varepsilon_i\psi_i(r) \quad (2\text{-}18)$$

While Hartree–Fock is a key method in quantum chemistry, it neglects electron correlation, which is addressed more effectively by methods such as DFT.

2.5. Density Functional Theory (DFT)

Density Functional Theory is one of the modern theories used in solid-state physics to study the electronic properties of materials. It was first introduced by Thomas and Fermi in 1927 through the Thomas-Fermi model, which relied on electronic density instead of the complex wave function. Later, Hohenberg and Kohn established a rigorous theoretical foundation for the theory in 1964, and it was developed further by Kohn and Sham in 1965. The theory gained wide application through computational programs such as Wien2k, developed in 1998.

The central idea of DFT is that the electronic density ρ(r) is sufficient to determine all electronic properties of a system without the need to know the complex wave function [5].

2.5.1. Hohenberg–Kohn Theorems

First Theorem: The electronic density ρ(r) uniquely determines the external potential $V_{ext}(r)$, and thus determines the full quantum state of the system.

Second Theorem: The total energy of the system can be expressed as a functional of the electronic density as follows:

$$E(\rho_0) = minE(\rho) \tag{2-19}$$

If the density function is exactly known:

$$E(\rho) = \langle\psi|H|\psi\rangle \tag{2-20}$$

The energy in Hohenberg–Kohn form is written as:

$$E_{H.K}(\rho) = \langle\psi|T + U|\psi\rangle \tag{2-21}$$

Where:

T: Kinetic energy of the electrons.

U: Electron-electron interaction potential.

Using the Hartree approximation, we obtain:

$$F_{H.K}(\rho) = \iint \frac{\rho(r)\rho(r\prime)}{|\vec{r}-\vec{r\prime}|} drdr' + G(\rho) \tag{2-22}$$

Where:

$G(\rho)$: It represents the kinetic energy of the electrons plus the difference between the true interaction energy and the Hartree interaction energy [1].

2.5.2. The Kohn–Sham Equations

To accurately compute the electronic density within Density Functional Theory (DFT), the Kohn–Sham equations are employed. These equations are based on the approximation that a many-electron interacting system can be mapped onto a system of non-interacting electrons moving in an effective potential [1, 2].

The electronic density is given by:

$$\rho(r) = \sum \psi_i^*(r)\,\psi_{i(r)} \quad (2\text{-}23)$$

The total electronic energy is expressed as:

$$E_e = T + V \quad (2\text{-}24)$$

Where:

T: The kinetic energy of the electrons.

V: The electron–electron interaction potential.

For practical computations, T is replaced by T_0, the kinetic energy of non-interacting electrons. An effective potential is introduced, incorporating the Hartree and exchange components. The energy is then written as:

$$E_{H.F} = T_0 + (V_H + V_X) \quad (2\text{-}25)$$

V_H: Hartree potential.

V_X: Exchange potential.

The exchange potential is defined as the difference between the actual potential and the Hartree potential:

$$V_X = V - V_H \quad (2\text{-}26)$$

The correlation potential is given by:

$$V_C = T - T_0 \quad (2\text{-}27)$$

Accordingly, the total energy functional becomes:

$$F_{H.K} = T + V + T_0 - T_0 = T_0 + V_H + (V_X + V_C) \quad (2\text{-}28)$$

The exchange–correlation potential is then defined as:

$$V_{XC} = V_X + V_C \quad (2\text{-}29)$$

Hence, the total energy of the system is expressed as:

$$E(\rho) = T_0(\rho) + V_H + V_{XC} + V_{ext}(\rho) \quad (2\text{-}30)$$

The Kohn–Sham equation is formulated as:

$$\left(T_0(\rho) + V_H(\rho) + V_{HC}(\rho) + V_{ext}(\rho)\right)\emptyset_i = \varepsilon_i \emptyset_i \quad (2\text{-}31)$$

2.5.3. Solving the Kohn–Sham Equation

Solving the Kohn–Sham equation requires choosing an appropriate basis set $\emptyset_\alpha$, allowing the wave function to be expressed in the following form [3]:

$$\psi_i = \sum C_{i\alpha}\, \emptyset_\alpha(r) \quad (2\text{-}32)$$

Where:

C_{ia}: are the expansion coefficients.

To determine the coefficients C_{ia}, the fundamental equations are solved using self-consistent iterations, ensuring that the total energy is minimized.

Thus, the Kohn–Sham solution takes the form:

$$(H - \varepsilon_i O)C_i = 0 \quad (2\text{-}33)$$

Where:

H: Kohn–Sham Hamiltonian.

O: Overlap matrix.

2.5.4. Exchange–Correlation Energy

The exchange–correlation energy represents a critical component in Density Functional Theory (DFT), as it encompasses the effects of both exchange and correlation interactions between electrons. These contributions cannot be independently calculated with high accuracy; hence, they are treated collectively.

2.5.4.1. Local Density Approximation (LDA)

In the LDA method, the exchange–correlation energy is approximated based on the assumption that the electron density at any point is equivalent to that of a uniform electron gas. Kohn and Sham (1965) introduced this approach, which expresses the exchange–correlation energy as [2]:

$$E_{XC}^{LDA}(\rho) = \int \rho(r)\varepsilon_{XC}\left(\rho(r)\right)dr^3 \quad (2\text{-}34)$$

Where $E_{XC}(\rho)$ is composed of:

$$E_{XC}(\rho) = \varepsilon_X(\rho) + \varepsilon_C(\rho) \quad (2\text{-}35)$$

$\varepsilon_X(\rho)$: Exchange energy.

$\varepsilon_C(\rho)$: Correlation energy.

The electron density is calculated from the Kohn–Sham orbitals as:

$$\rho(r) = \sum \psi_i^*(r)\psi_i(r) \quad (2\text{-}36)$$

2.5.4.2. Generalized Gradient Approximation (GGA)

The Generalized Gradient Approximation (GGA) is an improvement over the Local Density Approximation (LDA). It considers not only the electron density at each point but also the spatial gradient of this density ∇ρ(r). This allows for a more accurate representation of systems where the electron density is non-uniform, such as molecules and surfaces. The exchange–correlation energy in GGA is expressed as [3]:

$$E_{XC}^{GGA}(\rho) = \int \varepsilon_{XC}\big(\rho(r)\nabla\rho(r)\big)\, dr^3 \quad (2\text{-}37)$$

2.6. DFT Computational Software

Several computational packages have been developed for performing DFT calculations. These include [3]:

Free software: SIESTA, PWSCF, and ABINIT.

Paid software: VASP, CASTEP, and WIEN2k.

- **WIEN2k Software**

WIEN2k is one of the most accurate tools based on the Full-Potential Linearized Augmented Plane Wave method (FP-LAPW). The program is written in Fortran and runs on UNIX/Linux platforms. It is widely used in solid-state physics and materials science for investigating structural and electronic properties [6].

Main Applications of WIEN2k:

- Structural optimization and total energy minimization.

- Calculation of electronic properties using DFT with LDA or GGA functional.
- Extraction of exchange–correlation energies.
- Analysis of the electronic properties of RX-type compounds.
- Calculation and visualization of band structures and density of states (DOS).

Summary

In this chapter, we have introduced the theoretical framework of Density Functional Theory (DFT), focusing on the exchange–correlation energy and its approximation methods: LDA and GGA. These approximations allow for practical and accurate computation of electronic structures in real materials. Furthermore, we highlighted several DFT-based software tools, with particular emphasis on the WIEN2k program, known for its precision in simulating electronic properties. The chapter sets the foundation for computational modeling in the following sections of this study.

References

[1] Hohenberg, P., & Kohn, W. (1964). Inhomogeneous electron gas. *Physical review*, *136*(3B), B864.

[2] Kohn, W., & Sham, L. J. (1965). Self-consistent equations including exchange and correlation effects. *Physical review*, *140*(4A), A1133.

[3] Martin, R. M. (2020). *Electronic structure: basic theory and practical methods*. Cambridge university press.

[4] Szabo, A., and Ostlund, N. S., Modern Quantum Chemistry: Introduction to Advanced Electronic Structure Theory, Dover Publications, 1996.

[5] Parr, R. G. (1989). Density functional theory of atoms and molecules. In *Horizons of Quantum Chemistry: Proceedings of the Third International Congress of Quantum Chemistry Held at Kyoto, Japan, October 29-November 3, 1979* (pp. 5-15). Dordrecht: Springer Netherlands.

[6] Blaha, P., Schwarz, K., Madsen, G. K., Kvasnicka, D., & Luitz, J. (2001). wien2k. *An augmented plane wave+ local orbitals program for calculating crystal properties*, *60*(1), 155-169

Chapter 2 Density Functional Theory (DFT) and the WIEN2k Computational Program

Chapter 3:

Results and Discussion.

3.1. Introduction

The physical properties of lutetium hydride (LuH_2) were investigated using Density Functional Theory (DFT) as implemented in the WIEN2k software package. This program is based on the augmented plane wave plus local orbitals method to solve the Kohn-Sham equations. The exchange-correlation effects were treated using the Generalized Gradient Approximation (GGA)

3.2. Calculation method

3.2.1. Account configuration

In this study, the WIEN2k program was used to create a new project named LuH_2. All relevant information concerning the physical properties of the crystal structure was entered, including the identification of the atomic species of the compound, and selecting the type of crystal lattice, which in this case is face-centered cubic (FCC), where all angles are equal $\alpha = \beta = \gamma = 90°$. The lattice constant value (a) and the crystal symmetry group were also specified 225(Fm-3m).

Subsequently, the Xcrysden tool was employed to visualize the crystal structure of LuH_2, as illustrated in the following figure.

`

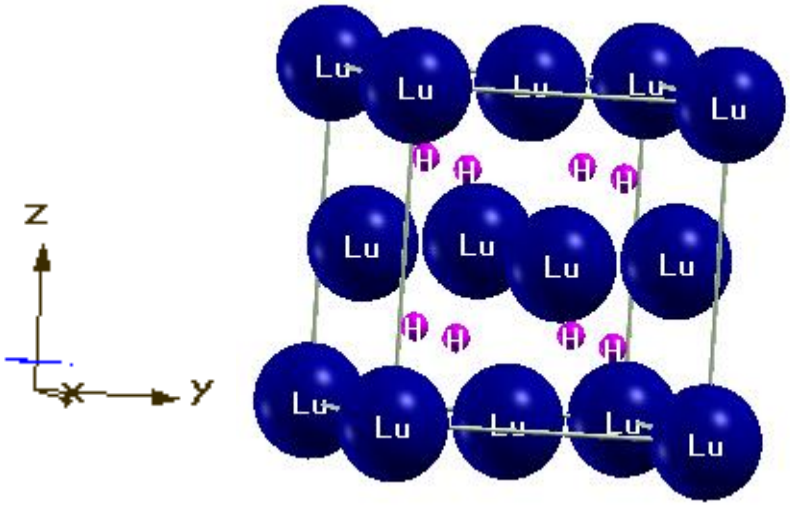

Figure (3-1): The crystal structure of LuH_2 using XcreysDen.

3.2.2. Initialization of parameters $R_{MTmin}*K_{max}$ and K-points

- **Firstly: $R_{MTmin}*K_{max}$**

In this part of the work, the value of $R_{MTmin}*K_{MAX}$ was gradually varied within the range from 5 to 9, while keeping both the lattice constant (a) and the number of k-points in the first Brillouin zone fixed.

Table (3-1): Variation of energy as a function of $R_{MTmin}*K_{max}$.

$R_{MTmin}*K_{max}$	Energy (Ry)
5	-29164.76958008
5.5	-29164.77576385
6	-29164.77770164
6.5	-29164.77837939
7	-29164.77858750
7.5	-29164.77866235
8	-29164.77868280
8.75	-29164.77868324
9	-29164.77868544

Here, R_{MTmin} represents the smallest atomic sphere radius in the studied unit cell, while K_{MAX} denotes the maximum wave vector modulus in the plane wave basis, corresponding to the lowest energy level considered in the calculations.

Table (3-1) and Figure (3-1) present the obtained results based on these variations, taking into account an energy convergence criterion set at 10^{-4} Ry to ensure calculation accuracy.

From the analysis of the Table (3-1) and Figure (3-1), the value of $R_{MTmin}*K_{max}=7.5$ was selected as the optimal parameter, given that the energy shows convergence and remains nearly constant at this point.

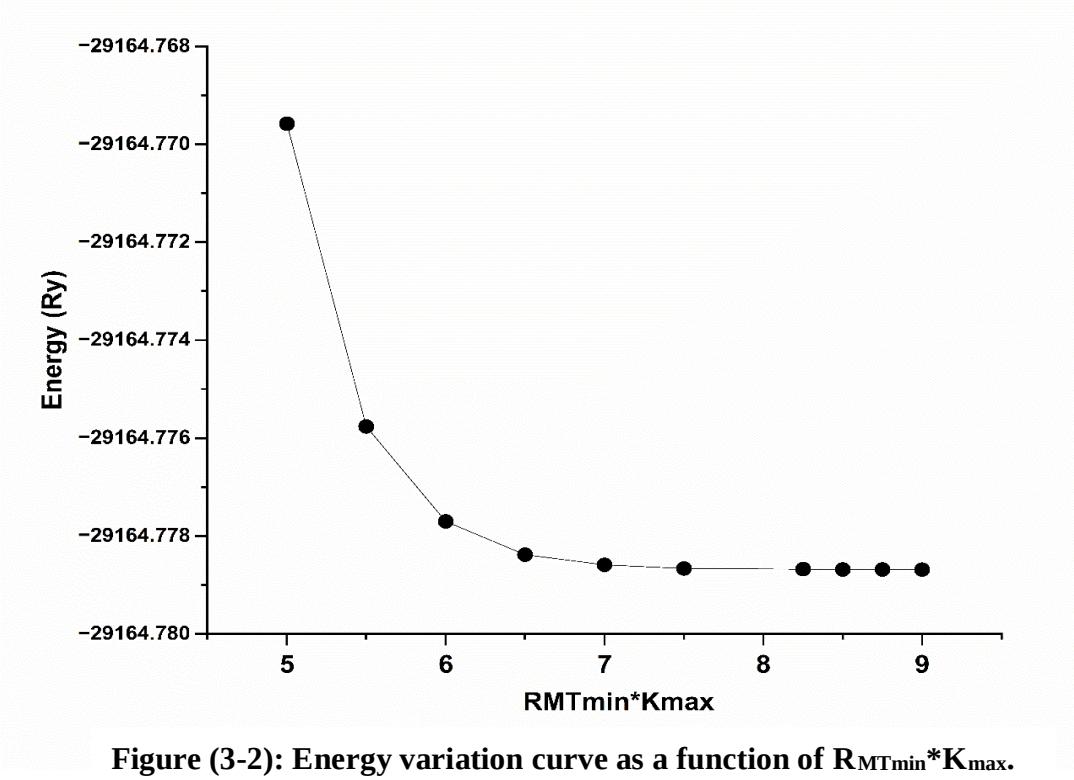

Figure (3-2): Energy variation curve as a function of R_{MTmin}*K_{max}.

- **Secondly: K-points**

After fixing the value of R_{MTmin}*K_{max} at 7.5, the number of K-points in the first Brillouin zone was varied. The Table (3-2) and Figure (3-2) below illustrate the results obtained from these variations.

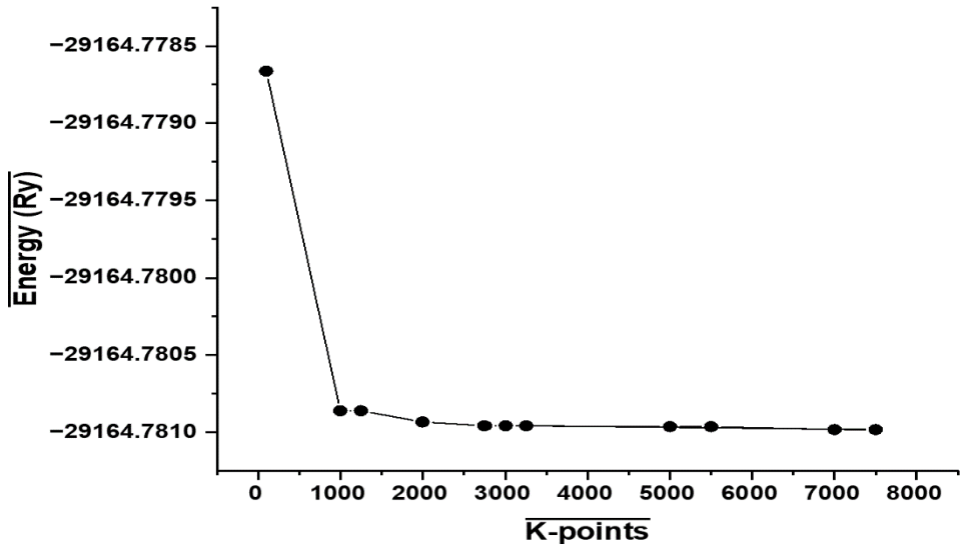

Figure (3-3): Energy variation curve as a function of K-points.

By analysing the Figure (3-3) and the Table (3-2), and following the same methodology used to determine the optimal value of $R_{MTmin}*K_{max}$, the optimal number of k-points was found to be 3000, as the total energy stabilizes at this value.

Table (3-2): Variation of energy as a function of K-points

K-points	Energy(Ry)
100	-29164.77866235
1000	-29164.78086121
1250	-29164.78086121
2000	-29164.78093462
2750	-29164.78095855
3000	-29164.78095855
3250	-29164.78095855
5000	-29164.78096440
5500	-29164.78096440
7000	-29164.78098378
7500	-29164.78098378

3.2.3. Cell size initialization results

Here, the lattice constant (a) was varied, effectively modifying the volume of the unit cell, while using the previously optimized values of $R_{MTmin}*K_{max}$ = 7.5 and k-points = 3000. The volume was altered over a defined range with an incremental step of 2%.

As a result, an energy–volume variation curve was obtained for LuH_2, as illustrated in the Figure (3-4). This curve allows us to extract information about the equilibrium volume of the unit cell by fitting it to a Murnaghan equation of state [1], which is given by the following expression:

$$E(V) = E_0 + \frac{B_0 V}{B_0'}\left(\frac{(V_0/V)^{B0'}}{B_0'-1} + 1\right) - \frac{B_0 V}{B_0'-1} \quad (3\text{-}1)$$

E_0: Total energy of the cell at equilibrium.

V_0: Equilibrium unit cell volume (stability).

B_0: Bulk modulus.

B_0': First derivative of the Bulk modulus with respect to the pressure.

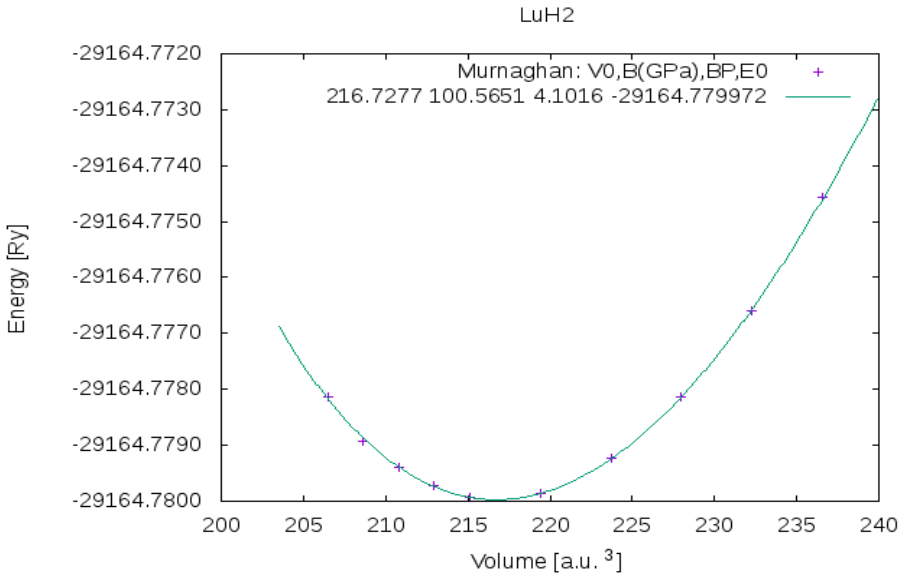

Figure (3-4): Total energy variation of LuH_2 with respect to the volume.

From the curve shown in Figure (3-4), it can be observed that the minimum energy value is: -29164.779972 Ry, corresponding to a volume of 216.7277 ($a.u^3$), which is referred to as the equilibrium cell volume. These results are presented in Table (3-3), along with some additional theoretical and experimental values available.

Table (3-3): Lattice parameter a_0(A°), bulk modulus B0(GPa), and the first derivative of the bulk modulus with respect to pressure B'(GPa) for lutetium dihydride (LuH_2), along with selected reference data

Compound	Calculation method	a_0(A°)	C(A°)	B_0(GPa)	B'(GPa)
LuH_2	The current study GGA	5.0458		100.5651	4.1016
LuH_2	[2]	5.033			
	Exp (T=298) [3]	5.0338			
LuH_{2+x}	at 295 K (x>0.9) [4]	3.558	6.443		
TmH_2	Exp [5]	5.09			
$YbH_{2.67}$	Exp [6] Space group P-31m (162)	6.3699(18)	9.007(5)		
ErH_2	[7]	5.1419		78.5587	4.6349

- The Table(3-3) shows a strong agreement between the calculated value and the available experimental and theoretical data. It is also observed that the lattice constant of LuH_2 is larger than that of LuH_{2+x}, indicating that increasing hydrogen concentration leads to a decrease in the lattice constant. This trend has also been observed in other rare-earth metal hydrides like GdH_x.[8], CeH_x [9], PuH_x [10] .Moreover, the compound changes its crystal structure from face-centred cubic (FCC) to hexagonal close-packed (HCP) due to the increased hydrogen concentration, where a = b ≠ c.

Table (3-4): Distances D between H-H, Lu-H, Lu-Lu atoms.

		$D_{(Lu-Lu)}$(Å)	$D_{(Lu-H)}$(Å)	$D_{(H-H)}$(Å)
LuH_2	The current study GGA	5.0458	2.1849	2.5229
TmH_2	[5]	5.6535	2.2120	2.5542

We observe that the atomic distances in TmH_2 are greater than in LuH_2, which indicates that as the atomic number (Z) increases, the distance between atoms decreases

3.3. Calculate of some physical properties of LuH_2

At this point, the optimized values previously obtained are used, corresponding to the stable state of the compound where $R_{MTmin}*K_{MAX}$=7.5, k-points=3000 and lattice constant a_0=5.0458 Å

3.3.1. Thermodynamic properties

At this phase, the formation energy of lutetium dihydride (LuH_2) ΔH_f is determined. It is calculated using the following relation:

$$\Delta H_f = E_{LuH2} - E_{Lu(hcp)} - E_{H_2} \quad (2\text{-}3)$$

Where:

E_{LuH2}: The total energy of LuH_2.

E_{hcpLu}: The total energy of lutetium in its hexagonal structure.

E_{H2}: The total energy of H_2 (as gas).

To gain deeper insight into the stability of lutetium dihydride, both the cohesive energy E_{coh} and the binding energy E_b (H) were calculated using the following two equation:

$$E_{coh}(LuH_2) = E_{LuH_2} - E_{Lu}^{atom} - 2E_H^{atom} \quad (3\text{-}3)$$

$$E_b(H) = \frac{1}{2}\left[E_{LuH_2} - E_{Lu(hcp)}\right] - E_H^{atom} \quad (3\text{-}4)$$

Where:

E_{Lu}^{atom}: Energy of the lutetium atom.

E_H^{atom}: Energy of the hydrogen atom.

Table (3-5): Heat of Formation ΔH_f (KJ/mol.H_2), average binding energy of the hydrogen atom E_b(H) (eV) and cohesive energy values of lutetium dihydride (LuH_2) Ecoh (eV) with comparison to the available reference data.

Compound		Eb(H)(eV)	Ecoh(eV)	ΔH_f (KJ/mol.H_2)
LuH_2	This study	-4.4342117852	-10.253406547	-209.819239352
TmH_2	[5]	-4.410910527	-10.89368283	-205.3297929

From Table (3-5), we observe the following:

- The heat of formation (ΔH_f) of LuH_2 is negative, indicating that lutetium dihydride can form spontaneously. This value lies within the range of formation energies of other rare-earth metal hydrides, as shown in the same Table.
- The average binding energy of the hydrogen atom E_b (H) in LuH_2 falls within the same range as that of TmH_2, suggesting similar bond strength and stability.
- The cohesive energy (E_{coh}) is also negative, indicating that LuH_2 is energetically stable.

3.3.2. Electronic properties

Electronic properties are the physical characteristics of a material that determine how it interacts with electrons or conducts electric current. These include conductivity, band structure, and density of states, Fermi energy, and more. They are fundamental to understanding the behavior of solid materials and their application in electronic devices [11].

3.3.2.1. Electronic Band Structure

The electronic band structure represents the distribution of allowed energy levels for electrons within solid materials. It arises from quantum interference among bonded atoms within a crystal lattice and explains the classification of materials as conductors, insulators, or semiconductors.

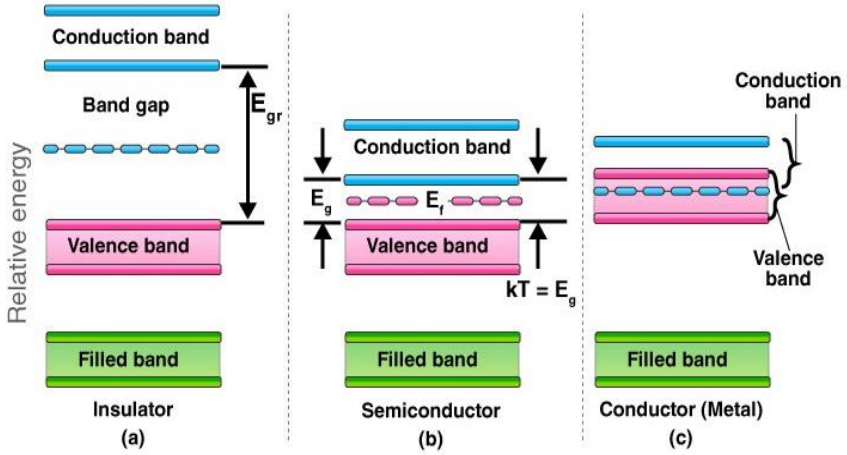

Figure (3-5): Energy band gaps in materials [12].

3.3.2.3. First Brillouin Zone

The first Brillouin zone is the Wigner-Seitz cell in reciprocal space and is used as a tool for analysing the energy distribution of electrons in periodic materials.

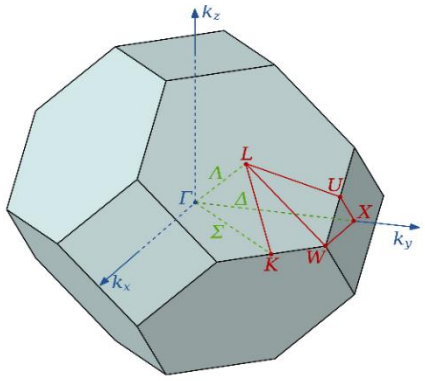

Figure (3-6): First brillouin zone of the FCC crystal lattice with high-symmetry points included [13].

The band structure is obtained by following specific paths that connect high-symmetry points within the first Brillouin zone of reciprocal space where are: L (1/2,1/2,1/2), K (3/8,3/8,3/4), w (1/2,1/4,3/4), X (1/2,0,1/2), Γ (0,0,0) (as shown in Figure (3-6)). This structure represents the distribution of electronic energy levels, ranging from the lowest to

the highest energies, as a function of the wave vector. The resulting diagram illustrates the band structure of lutetium dihydride (LuH_2), where the curves describe the relationship between electron energy and the wave vector in reciprocal space.

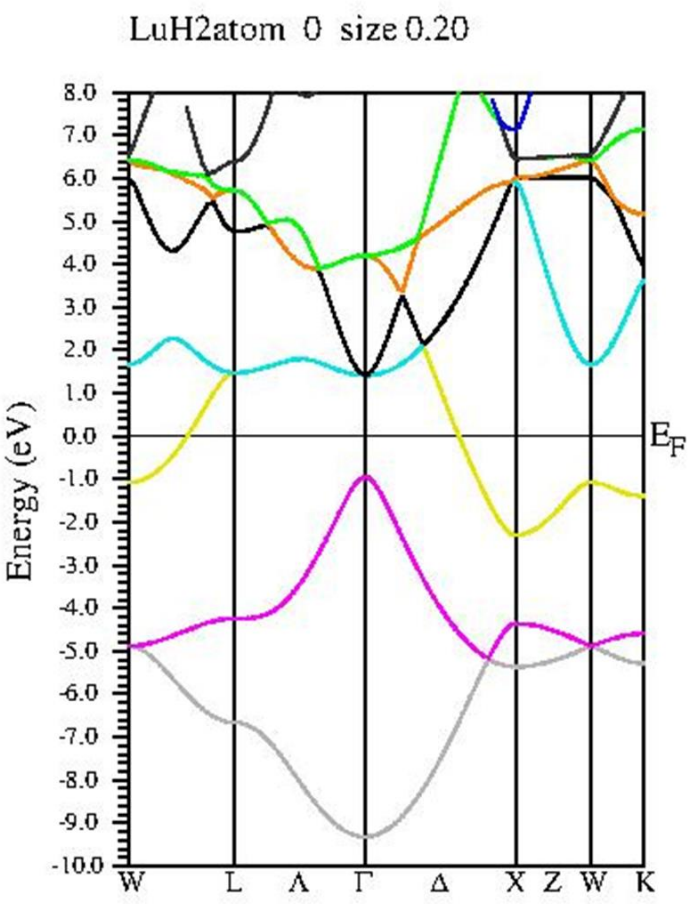

Figure (3-7): Band structure of LuH_2

As observed in Figure (3-7), some bands cross the Fermi level, and no band gap is present E_g=0 (ev), indicating that LuH_2 exhibits metallic behavior.

3.3.2.4. Total and partial density of States (DOS)

The density of states refers to the number of available electronic states at each energy level. It is used to interpret the electronic and thermal behavior of materials.

To identify the electronic states that contribute to the formation of the valence and conduction bands in the studied compound, both the total and partial density of states (DOS) are analyzed. This analysis provides insight into the nature of the atomic orbitals involved in the electronic behavior of the material.

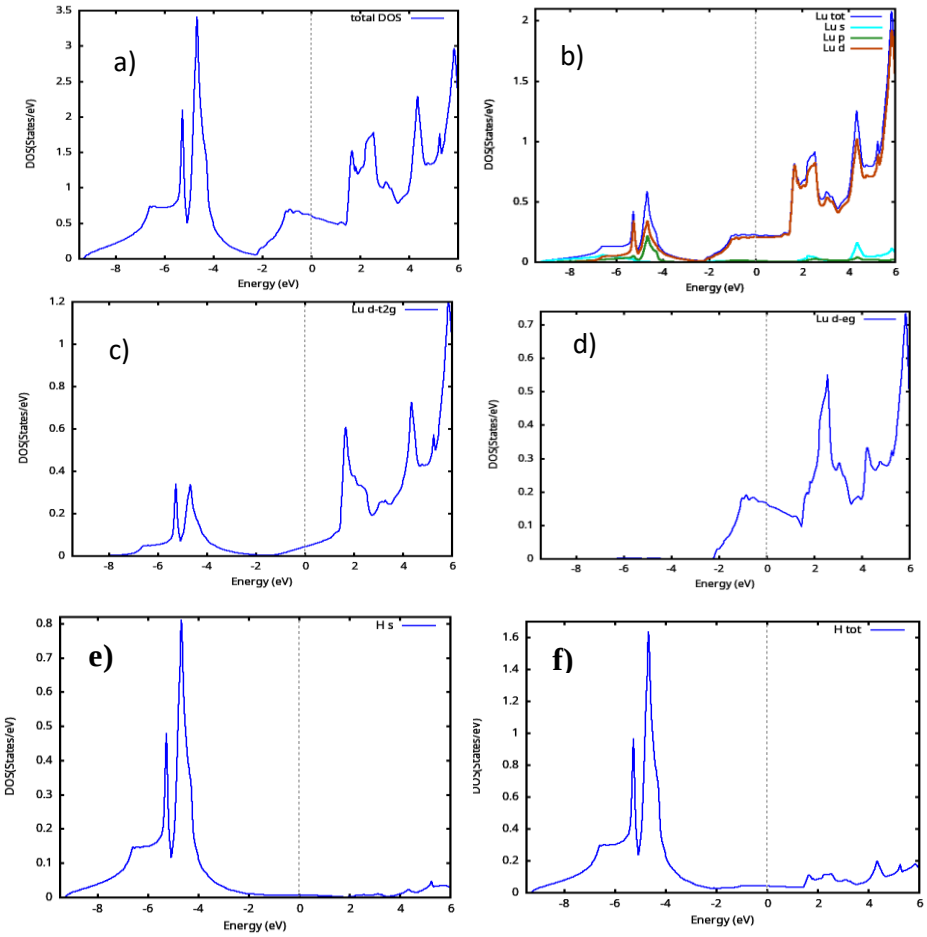

Figure (3-8): Total and partial density of States (DOS) of the hydrides: a) Total density of states of lutetium dihydride, b)total density of states of Lu atom and Lu-s-p-d orbitals, c) partial density of states of Lu-d-t2g orbital, d) partial density of states of Lu-d-eg orbital, e) partial density of states of s orbital of H atom, f) Total density of states of H.

The partial density of states represents the distribution of electron energies associated with a specific atom and its atomic orbitals (s, p, d). It indicates the number of available electronic states per unit of energy (eV) and serves as an essential tool for understanding the contribution of each orbital type to the overall electronic structure of the material.

When ligands approach a central metal ion, they exert an uneven effect on the five d orbitals, resulting in what is known as "d-orbital splitting." This occurs because the lone electron pairs on the ligands repel the electrons in the d orbitals. The orbitals aligned directly along the ligand axes experience greater repulsion and thus increase in energy, while those positioned between the axes are less affected and remain at lower energy. This interaction causes the d orbitals to split into two energy levels, separated by an energy gap. This phenomenon is fundamental for understanding the electronic, optical, and magnetic behaviour of transition metal complexes [14].

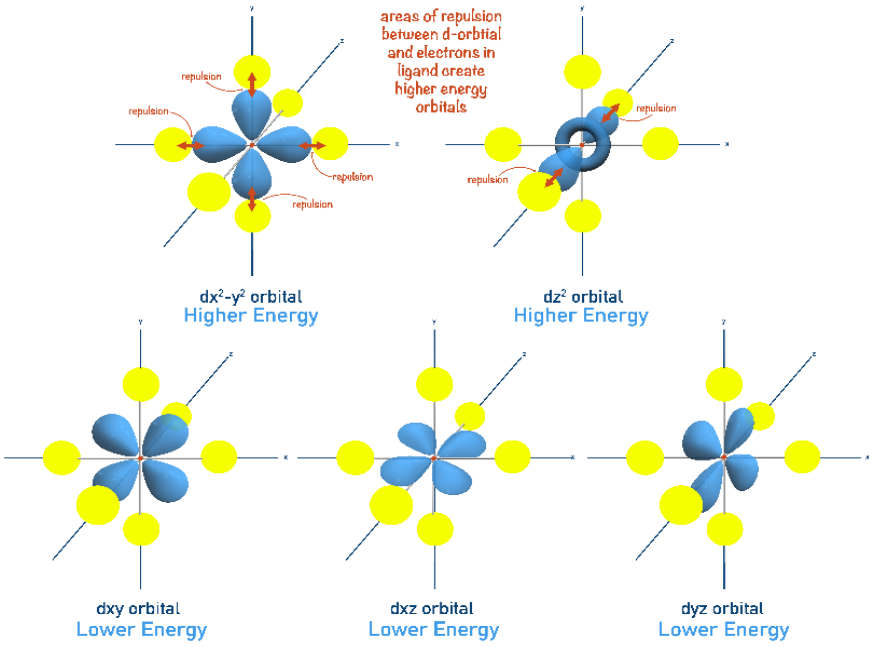

Figure (3-9): Illustration of the splitting of d orbitals into two groups upon the approach of ligands to the central metal ion [14].

Table (3-6): Fermi energy E_F(Ry), total and partial density of states (states/ev)for the atomic states s, p, d eg, dt2g of Lu and the s state of H.

	LuH_2
E_F(Ry)	0.54027
N_F(EF)	8.33
NF(Lu-tot)	3.07
NF(Lu-s)	0.02

NF(Lu-p)	0.15
NF(Lu-d)	2.86
NF(Lu-d-eg)	2.27
NF(Lu-d-t2g)	0.59
NF(H-tot)	0.56
NF(H-s)	0.09

The calculated total density of states for lutetium dihydride is illustrated in the accompanying Figure (3-8). Based on this figure and the data presented in Table (3-6), it is evident that the density of states at the Fermi level is non-zero, indicating that the compound exhibits metallic behaviour. This finding is consistent with the conclusions previously drawn from the band structure analysis.

3.3.3. Elastic properties

Elastic properties describe a material's ability to return to its original shape after the removal of an applied force. Within the elastic range, the relationship between stress and strain is linear, and the material obeys Hooke's Law. The elastic modulus, defined as the ratio of stress to strain, serves as a measure of the material's resistance to deformation [15].

- **Stress tensile**

Stress refers to the internal force experienced by a material per unit area when an external force is applied. It describes how particles within a solid exert forces on one another in response to loading [16].

- **Strain tensile**

Strain is a dimensionless measure of deformation that quantifies the relative displacement between particles in a material compared to their original length. It indicates how much a material stretches or compresses under stress.

Robert Hooke was the first to study the relationship between stress and strain in elastic material. The fundamental laws governing the mechanical behavior of materials are expressed by the following relations [17]:

$$\delta_{ij} = \sum_{k,l} c_{ijkl}\, \varepsilon_{kl} \tag{3-5}$$

The stress and strain tensors are related through the following expression:

$$[\delta] = \begin{bmatrix} \delta_1 & \delta_6 & \delta_5 \\ \delta_6 & \delta_2 & \delta_4 \\ \delta_5 & \delta_4 & \delta_3 \end{bmatrix} = \begin{bmatrix} \delta_1 \\ \delta_2 \\ \delta_3 \\ \delta_4 \\ \delta_5 \\ \delta_6 \end{bmatrix} \tag{3-6}$$

$$[\varepsilon] = \begin{bmatrix} \delta_1 & \frac{1}{2}\varepsilon_6 & \frac{1}{2}\delta_5 \\ \frac{1}{2}\varepsilon_6 & \varepsilon_2 & \frac{1}{2}\varepsilon_4 \\ \frac{1}{2}\varepsilon_5 & \frac{1}{2}\varepsilon_4 & \varepsilon_3 \end{bmatrix} = \begin{bmatrix} \varepsilon_1 \\ \varepsilon_2 \\ \varepsilon_3 \\ \varepsilon_4 \\ \varepsilon_5 \\ \varepsilon_6 \end{bmatrix} \tag{3-7}$$

To describe the elastic constants c_{ij}, we use the properties of matrix multiplication:

$$\begin{pmatrix} \delta_1 \\ \delta_2 \\ \delta_3 \\ \delta_4 \\ \delta_5 \\ \delta_6 \end{pmatrix} = \begin{pmatrix} C_{11} & C_{12} & C_{13} & C_{14} & C_{15} & C_{16} \\ C_{12} & C_{22} & C_{23} & C_{24} & c_{25} & C_{26} \\ C_{13} & C_{23} & C_{33} & C_{34} & C_{35} & C_{36} \\ C_{14} & C_{24} & C_{34} & C_{44} & C_{45} & C_{46} \\ C_{15} & C_{25} & C_{35} & C_{45} & C_{55} & C_{56} \\ C_{16} & C_{26} & C_{36} & c_{46} & C_{56} & C_{66} \end{pmatrix} = \begin{pmatrix} \varepsilon_1 \\ \varepsilon_2 \\ \varepsilon_3 \\ \varepsilon_4 \\ \varepsilon_5 \\ \varepsilon_6 \end{pmatrix} \tag{3-8}$$

In cubic crystal systems, the high degree of symmetry reduces the number of independent elastic constants from 21 (in the general case) to only three: C_{11}, C_{12} and C_{44}. This simplification is a direct result of the symmetry constraints, which lead to equal or vanishing components in the elastic stiffness matrix [18].

The elastic constants C_{ij} for the cubic structure are given by the following matrix:

$$(C_{ij}) = \begin{pmatrix} C_{11} & C_{12} & C_{12} & 0 & 0 & 0 \\ C_{12} & C_{11} & C_{12} & 0 & 0 & 0 \\ C_{13} & C_{12} & C_{11} & 0 & 0 & 0 \\ 0 & 0 & 0 & C_{44} & 0 & 0 \\ 0 & 0 & 0 & 0 & C_{44} & 0 \\ 0 & 0 & 0 & 0 & 0 & C_{44} \end{pmatrix} \quad (3\text{-}9)$$

$$= \begin{pmatrix} 141.810 & 60.651 & 60.651 & 0 & 0 & 0 \\ 60.651 & 141.810 & 60.651 & 0 & 0 & 0 \\ 60.651 & 60.651 & 141.810 & 0 & 0 & 0 \\ 0 & 0 & 0 & 93.608 & 0 & 0 \\ 0 & 0 & 0 & 0 & 93.608 & 0 \\ 0 & 0 & 0 & 0 & 0 & 93.608 \end{pmatrix} \quad (3\text{-}10)$$

Where:

$$C_{11} = \frac{s_{11}+s_{12}}{(s_{11}-s_{12})(s_{11}+2s_{12})} \quad (3\text{-}11)$$

$$C_{12} = \frac{-s_{12}}{(s_{11}-s_{12})(s_{11}+2s_{12})} \quad (3\text{-}12)$$

$$C_{44} = \frac{1}{s_{44}} \quad (3\text{-}13)$$

There are several elastic constants for the crystal, including:

- **Elastic anisotropy factor A:**

It refers to the directional dependence of mechanical properties in crystalline materials, such as Young's modulus and acoustic velocity. This non-uniform response to stress or strain is rooted in crystallographic orientation and plays a significant role in material failure, particularly in the formation and growth of microcracks. It is commonly quantified using indicators like the Zener ratio for cubic crystals or the universal elastic anisotropy index for other crystal systems [19]. It is given by the following relation:

$$A = \left(\frac{2C_{44}}{C_{11}-C_{12}}\right) \quad (3\text{-}14)$$

- **Bulk modulus B:**

The bulk modulus is a measure of a material's resistance to volume change when subjected to uniform pressure from all directions [20] and it is expressed by the equations:

$$B_R = B_V = \frac{1}{3}(C_{11} + 2C_{12}) \quad (3\text{-}15)$$

$$B = B_H = \frac{1}{2}(B_R + B_V) = \frac{1}{3}(C_{11} + 2C_{12}) \quad (3\text{-}16)$$

- **Shear modulus G:**

Shear modulus measures a material’s resistance to deformation under shear stress and is defined as the ratio of shear stress to shear strain. For polycrystalline materials, it is estimated using the Voigt, Reuss, and Hill approximations, which provide a realistic average based on theoretical bounds [21, 22].

Voigt approximation:

$$G_V = (C_{11} - C_{12} + 3C_{44})\frac{1}{5} \quad (3\text{-}16)$$

Reuss approximation:

$$G_R = \frac{5(C_{11}-C_{12})C_{44}}{4C_{44}+3(C_{11}-C_{12})} \quad (3\text{-}17)$$

Thus, we find:

Hill approximation:

$$G_H = (G_R + G_V)\frac{1}{2} \quad (3\text{-}18)$$

- **Stiffness:**

Stiffness is a property that describes a material's ability to resist deformation when subjected to an external force. In other words, it refers to the amount of force required to produce a unit displacement or strain. The stiffer a material is, the more force is needed to deform it.

Stiffness is commonly quantified using Young's modulus, which relates stress to strain within the elastic region [23].

- **Young's modulus E:**

Young's modulus is a measure of a material's elasticity, describing the relationship between stress and strain in the linear portion of a material's deformation under tensile or compressive forces. It quantifies how much a material resists length changes when subjected to stress. Materials with a high Young's modulus are stiff and resist deformation [24].

It is given by the following relation:

$$E = \frac{9GB}{3B+G} \tag{3-19}$$

- **Poisson's ratio δ_H:**

Poisson's ratio is a physical quantity that describes the ratio of transverse strain to axial strain in a material subjected to tension or compression. It indicates how much a material contracts laterally when stretched longitudinally. Materials with a higher Poisson's ratio exhibit more lateral contraction [24].

It is given by the following relation:

$$\delta = \frac{1}{2}\left[\frac{3B-2G}{3B+G}\right] \tag{3-20}$$

Based on Young's modulus and Poisson's ratio, the Lamé parameters, which characterize the stiffness of a material, can be calculated.

$$\mu = \frac{E}{2(1+\delta)} \tag{3-21}$$

$$\lambda = \frac{\delta E}{(1+\delta)(1-2\delta)} \tag{3-22}$$

- **Hardness:**

Hardness refers to a material's resistance to plastic deformation, such as denting, scratching, or indentation. It reflects how well a material can withstand localized mechanical forces without undergoing permanent shape change. For instance, diamond exhibits extremely high hardness, making it very difficult to scratch or deform, whereas most plastics are relatively soft and easily indented or scratched. As illustrated in comparative scales, hardness spans from soft materials like plastics to exceptionally hard substances like diamond, with most other materials falling in between [25].

- **Vickers hardness:**

Vickers hardness is a measure of a material's resistance to plastic deformation. It can be theoretically estimated using semi-empirical models such as the Chen and Tian models, which rely on elastic parameters.

- **Chen's model:**

Chen's model is a semi-empirical approach used to estimate the Vickers hardness of solid materials based on the shear modulus and Pugh's ratio. It offers a simple yet effective method to predict the hardness of polycrystalline materials and is given by [26]:

$$H_V^{chen} = 2(K^3G)^{0.585} - 3, (k = G/B) \quad (3\text{-}23)$$

- **Tian's model:**

Tian's model is an improved theoretical model for predicting Vickers hardness, incorporating both the shear modulus and Pugh's ratio more accurately. It is particularly suitable for ductile materials and is expressed as [27]:

$$H_V^{Tian} = 0.92\left(\frac{G}{B}\right)^{1.137} G^{0.708} \quad (3\text{-}24)$$

We utilized the IRelast package integrated with WIEN2k to calculate the elastic constants (C_{ij}) and determine various mechanical properties, including Young's modulus (E), shear modulus (G), elastic anisotropy index (A), bulk modulus (B), Poisson's ratio δ_H, Lamé parameters, as well as Chen and Vickers hardness values H.

The obtained results are summarized in Table (3-7).

Table (3-7): Elastic constants c_{ij} (GPa), Young's modulus E (GPa), shear modulus G (GPa), elastic anisotropy factor A, poisson's ratio δ_H (GPa), Lamé parameters μ, λ (GPa), Chen-Vickers hardness H (GPa), Bulk modulus B.

	LuH_2	YbH_2
	GGA	[28]
C_{11}	141.810	97.583
C_{12}	60.651	42.01
C_{44}	93.608	52.015
E_H	160.082	82.097
G_H	66.936	33.97
δ_H	0.196	
B	87.704	46.91
B/G (Pugh' Ratio)	1.310	1.38
A	2.3068	1.87
λ	43.080	
μ	66.936	
H (Chen-Vickers hardness)	14.05	

The elastic constants C_{11}, C_{12}, and C_{44} are fundamental parameters for assessing the mechanical stability of crystals with cubic symmetry. To satisfy the mechanical stability conditions, these constants must fulfill the Born–Huang criteria [29], expressed as follows:

$$C_{11} - C_{12} = 81.159 > 0$$

$$C_{11} + 2C_{12} = 263.112 > 0$$

$$C_{44} > 0$$

According to the calculated results, all these conditions are satisfied for lutetium hydride, clearly indicating that this compound is mechanically stable.

Based on the results presented in Table (3-7), the following observations can be made:

- The value of C_{44} is significantly smaller than that of C_{11}, indicating that LuH_2 is easily deformable.
- The anisotropy factor A is greater than 1, suggesting that this compound exhibits pronounced elastic anisotropy.
- The bulk modulus B lies between C_{11} and C_{12}, which confirms the elastic stability of the compound.

According to the empirical criterion proposed by Pugh (1954), the ductile or brittle behavior of materials can be evaluated by the ratio of the bulk modulus (B) to the shear modulus (G). Materials with a B/G ratio greater than 1.75 are typically classified as ductile, while those with lower values are considered brittle [30]. Based on the results reported in Table (3-7), the calculated B/G ratio is less than 1.75, indicating that LuH_2 is classified as a brittle material.

Based on the value of Poisson's ratio, it is possible to infer the nature of atomic bonding in a material. A value close to 0.10 typically indicates covalent bonding, while a value near 0.25 suggests ionic bonding [31]. In this study, the calculated Poisson's ratio is 0.196, which falls between these two limits. This suggests that bonding in LuH_2 exhibits a mixed character between covalent and ionic.

We calculate the Debye $\theta_D$temperature based on the average sound velocity V_m using the following equation [32]:

$$\theta_D = \frac{h}{K_B}\left[\frac{3n}{4\pi V_a}\right]^{\frac{1}{3}} V_m \qquad (3\text{-}24)$$

Where:

- h: Plank's constant.
- K_B: Boltzman's constant.
- V_a: Atomic volume.
- n: Number of atoms per unit volume.
- V_m: Average sound velocity expressed as follows:

$$V_m = \left[\frac{1}{3}\left(\frac{2}{V_t^3} + \frac{1}{V_l^3}\right)\right]^{\frac{-1}{3}} \quad (3\text{-}25)$$

- V_l: Longitudinal wave velocity [33].

$$V_l = \left(\frac{3B+4G}{3\rho}\right)^{1/2} \quad (3\text{-}26)$$

- V_t: Transverse wave velocity [34, 35].

$$V_t = \left(\frac{G}{\rho}\right)^{\frac{1}{2}} \quad (3\text{-}27)$$

ρ: Volumetric density.

- T_m: Melting temperature [36].

$$T_m = 553 + 5.91C_{11}$$

Based on the data presented in Table (3-8), it can be concluded that longitudinal waves propagate more efficiently than transverse waves. Moreover, the material can be utilized at high temperatures due to its high melting point.

Table (3-8): Average velocity V_m (m/s), transverse velocity V_t (m/s), longitudinal velocity of sound waves V_l (m/s), melting temperature T_m (K) and Debye temperature $\theta_D(K)$.

		$\rho(g/cm^3)$	V_l(m/s)	V_t(m/s)	V_m(m/s)	T_m(K)	$\theta_D(K)$
LuH_2	This study	9.1588	4397.428	2704.584	2984.471	1391.0971	403.160
TmH_2	[5]	8.5179	3768.14	2246.67	2486.88	1186.9491	331.824
YbH_2	[2]					1129	299.45

3.3.4. Optical properties

Optical properties of materials refer to how they interact with light, including reflection, refraction, absorption, and transmission. These properties determine the behavior of light as it passes through or reflects off a material, influencing various optical applications [37].

- **Electrical insulation function**

The electrical insulation function $\varepsilon(\omega)$ (also known as the dielectric function) is given by the following relation [37]:

$$\varepsilon(\omega) = \varepsilon_1(\omega) + i\varepsilon_2(\omega) \quad (3\text{-}28)$$

ε_1: The real part represents the material's absorption behavior.

ε_2: The imaginary part is associated with the material's polarization response.

The imaginary part of the equation is given by the following form:

$$\varepsilon_2(\omega) = \frac{e^2\hbar}{\pi m^2\omega^2} K \sum VC \int |M_{CV}(K)|^2 [M_{CV}(K) - \omega] d^3 \quad (3\text{-}29)$$

The integral over the entire first Brillouin zone is given by the following expression:

$$M_{CV}(K) = \langle U_{ck}|e\nabla|U_{ck}\rangle \quad (3\text{-}30)$$

It corresponds to the components of the dipole moment matrix elements of electrons and is defined as the vector potential of the electric field.

U_{ck}: Transition matrix elements from the conduction band to the valence band.

The expression for energy in this case is given by:

$$\hbar\omega_{CV} = E_{CK} - E_{VK} \quad (3\text{-}31)$$

This equation corresponds to the transition energy between the two bands.

The relationship between the real and imaginary parts of the dielectric function is given by the Kramers–Kronig relation [38].

$$\varepsilon_1(\omega) = 1 + \frac{2}{\pi} P \int_0^\infty \frac{\omega\prime\varepsilon_2(\omega\prime)}{\omega\prime^2 - \omega^2} d\omega' \quad (3\text{-}32)$$

Where:

P: Principal value of the integral

$\varepsilon_1, \varepsilon_2$: They are used to calculate the refractive index , which is given by the following relation:

$$n(\omega) = \left[\frac{\varepsilon_1(\omega)}{2} + \frac{\sqrt{\varepsilon_1^2(\omega)+\varepsilon_2^2(\omega)}}{2}\right]^{\frac{1}{2}} \quad (3\text{-}33)$$

By knowing the real and imaginary parts of the dielectric function, several other optical properties can be derived, such as reflectivity, optical conductivity, refractive index, absorption coefficient, and attenuation coefficient.

We used the Generalized Gradient Approximation (GGA) to calculate the optical properties. By launching the WIEN2k program and selecting "optics" from the Tasks menu, we access the optical properties window. After clicking all the required buttons sequentially, and in order to obtain the dielectric function $\varepsilon(\omega)$, we select luh2 joint, resulting in the two curves shown in Figures below:

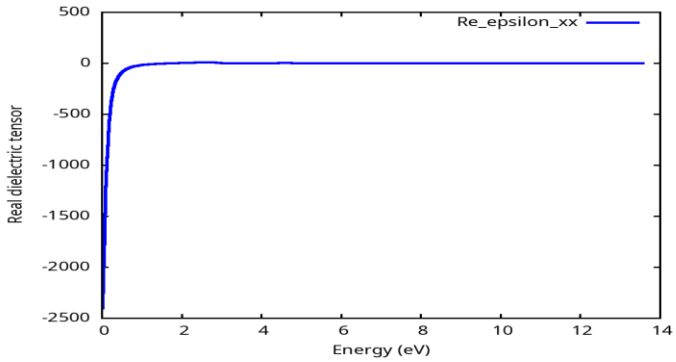

Figure (3-10): The real dielectric constant

It can be observed from the curve in Figure (3-10) that the real part of the dielectric function exhibits a negative value in the energy range from 0.01361eV to 1.75513 eV. This indicates that incident photons are fully absorbed within the optical medium in this range, revealing a metallic behavior of the material.

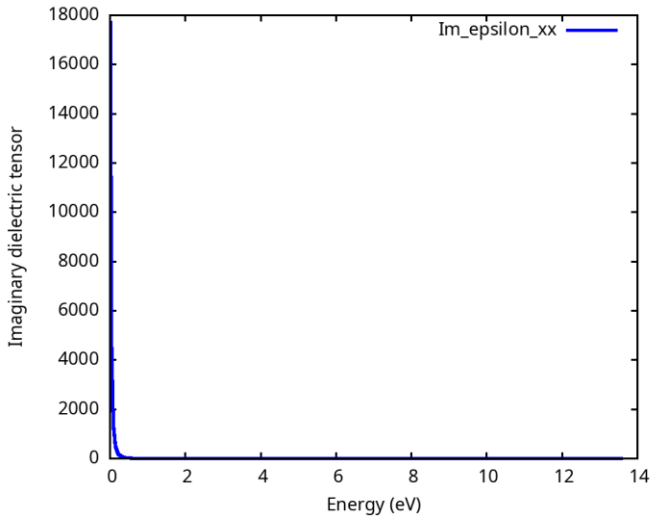

Figure (3-11): The imaginary dielectric constant curve.

From the curve in Figure (3-11), it is observed that the imaginary part of the dielectric constant reaches a peak value of approximately 17713.1, then sharply decreases until it becomes negligible. This behavior indicates that this dihydride acts as a transparent material in the high-energy region.

- **Optical conductivity $\sigma(\omega)$:**

Optical conductivity is the ability of a material to absorb photons as a result of electron transitions from the valence band to the conduction band when exposed to light or an alternating electric current. It is typically derived from the imaginary part of the dielectric function. It is given by the following equation [37]:

$$\sigma(\omega) = \frac{\omega}{4\pi} Im\varepsilon(\omega) \qquad (3\text{-}34)$$

The optical conductivity is illustrated in Figures (3-12) and (3-13):

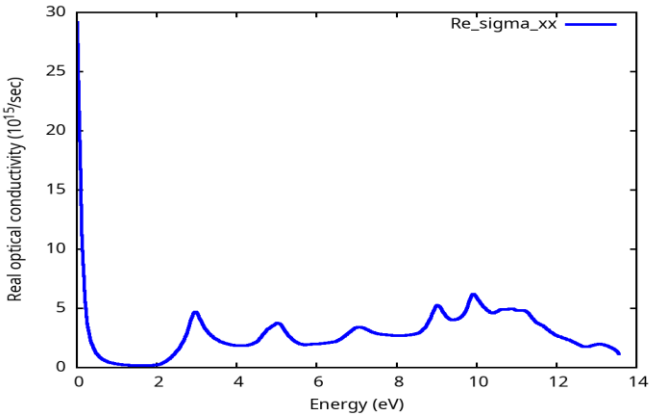

Figure (3-12): The real optical conductivity curve

From the curve in Figure (3-12), it is evident that the real part of the optical conductivity reaches its maximum at 0.01361 eV, then drops to zero in the energy range between 1.53744 and 1.78235 eV, and subsequently begins to increase again.

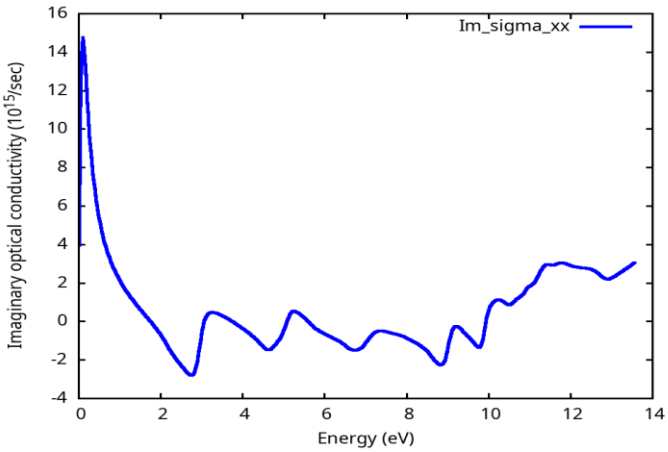

Figure (3-13): The optical imaginary conductivity curve

From the curve in Figure (3-13), it is observed that the imaginary part of the optical conductivity reaches a maximum (14.7522) at a certain energy 0.09524 eV, then gradually decreases while exhibiting small oscillations.

- **Absorption coefficient $\alpha(\omega)$:**

The absorption coefficient is a physical quantity used to measure how effectively a material absorbs electromagnetic waves, particularly light. It quantifies the decrease in light intensity as it passes through a material due to the absorption of photons. This absorption is typically associated with electronic transitions from the valence band to the conduction band and depends on the angular frequency of the incident light.

The absorption coefficient can be calculated from the complex dielectric function using the following expressions [37]:

$$\alpha(\omega) = \frac{2\pi}{\lambda} K(\omega) \tag{3-35}$$

λ: The wavelength of light in vacuum.

$$\alpha(\omega) = \frac{2\pi\omega}{C} \sqrt{\frac{-Re\varepsilon(\omega)|\varepsilon(\omega)|}{2}} \tag{3-36}$$

The absorption coefficient is represented in the figure:

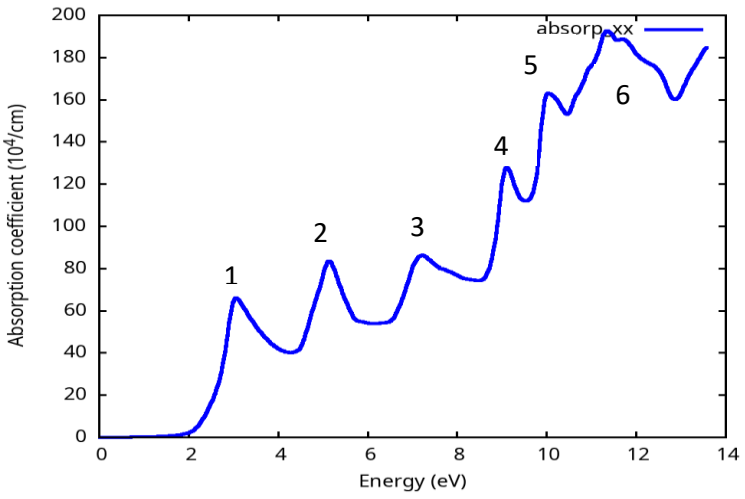

Figure (3-14): The absorption coefficient curve

Table (3-9): The energy values of each absorption coefficient peak and their corresponding wavelengths.

The peak	Energy (eV)	The wavelength (nm)
1	3.06128	405.04830
2	5.12935	241.74407
3	7.22463	171.62125
4	9.10221	136.25887
5	10.0274	123.64168
6	11.360760	109.19619

From the analysis of curve (3-14) and table (3-9), it is evident that the first peak in the absorption spectrum lies within the visible light range, specifically in the violet region, with a wavelength of approximately 405 nm. The other peaks fall within the ultraviolet spectrum, which includes wavelengths shorter than 400 nm. It can be inferred that the absorption nature is strong in the spectral regions spanning the range of all studied wavelengths. Therefore, this compound can also be utilized as an effective filter for different energy levels in the ultraviolet spectrum.

- **Refractive index n (ω), extinction coefficient k (ω):**

The refractive index (n) is a measure of how much the speed of light is reduced when passing through a given material compared to its speed in a vacuum. It also represents the change in the direction of a light ray as it passes from one medium to another, as described by Snell's Law. It is expressed by the equation [37]:

$$n\,(\omega) = \left[\frac{\varepsilon_1(\omega)}{2} + \frac{\sqrt{\varepsilon_1^2(\omega)+\varepsilon_2^2(\omega)}}{2}\right]^{\frac{1}{2}} \qquad (3\text{-}37)$$

The refractive index is illustrated in the figure (3-15):

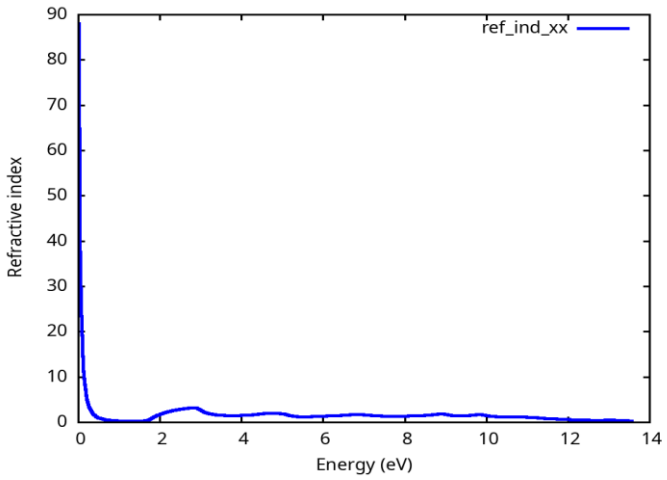

Figure (3-15): The refractive index curve.

From Figure (3-15), it is observed that the refractive index reaches a value of 87.9521 at the energy 0.01361 eV, then gradually decreases until it becomes zero within the range 0.80274-1.70071 eV. A slight increase is then noted, followed by small, damped oscillations that eventually tend to zero.

The imaginary part of the complex refractive index, known as the extinction coefficient, is given by the relation:

$$k\ (\omega) = \left[\frac{-\boldsymbol{\varepsilon_1(\omega)}}{2} + \frac{\sqrt{\varepsilon_1^2(\omega)+\varepsilon_2^2(\omega)}}{2}\right]^{\frac{1}{2}} \quad (3\text{-}38)$$

- **Reflection coefficient:**

The reflectivity is defined as the ratio between the intensity of the reflected light and that of the incident light on the surface of a material. It is expressed by the following relation [39]:

$$R(\omega) = \frac{(n-1)^2+k}{(n-1)^2+k} \quad (3\text{-}39)$$

The reflectivity is illustrated in Figure (3-16):

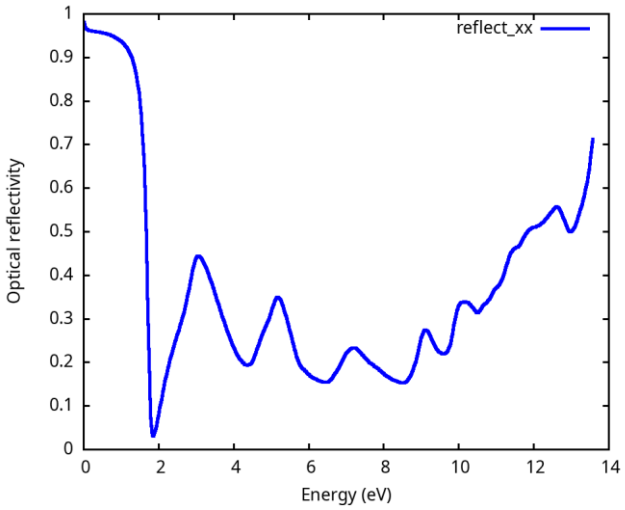

Figure (3-16): The reflectivity curve.

From the curve in Figure (3-16), it is observed that the reflectivity reaches its maximum value of 0.980512 within the energy range 0.01361 eV, then gradually decreases until it reaches a value of 0,031386 at energy 1.86398 eV, after which it starts to increase again.

Conclusion

In this chapter, we focused on investigating various physical properties of lutetium hydride (LuH_2) through theoretical calculations using the Wien2k simulation software. The study encompassed structural, thermodynamic, electronic, and optical characteristics.

The analysis began with examining the structural properties at absolute zero temperature (0K), where all of the lattice constant, formation energy, binding energy and cohesive energy were determined. The results revealed a notable energetic stability of the compound, suggesting its feasibility of synthesis due to its relatively low formation energy compared to similar materials.

Regarding the electronic properties, the band structure showed a clear overlap between the valence and conduction bands at the Fermi level, which indicated that LuH_2 behaves as a metallic compound. Moreover, the density of states analysis highlighted significant contributions from lutetium d-orbitals, especially from the Lu-d-eg sub-levels at the Fermi energy.

On the mechanical side, the primary elastic constants c11, c12, and c44 were computed. The obtained values demonstrated that the compound possesses good elasticity and mechanical behaviour, indicating that it can undergo deformation easily without structural failure, thus classifying it as a brittle and mechanically stable material.

As for the optical properties, both the real and imaginary parts of the dielectric function were evaluated, along with the reflectivity R (ω), refractive index n (ω), optical conductivityσ (ω), and absorption coefficient$\alpha(\omega)$. The results showed that the compound exhibits a wide optical response over the energy range from 0 to 14 eV, which makes it a promising candidate for optical applications, particularly in the ultraviolet region.

References

[1] Murnaghan, F. D. (1944). The compressibility of media under extreme pressures. *Proceedings of the National Academy of Sciences*, *30*(9), 244-247.

[2] Saidi, F., Mokhdar, S., Dergal, M., Mahmoudi, A., Kallekh, A., & Abd El-Gawad, H. H. (2023). Ab initio study of the structural, electronic, magnetic, mechanical, optical, and dynamical properties of the rare-earth dihydrides MH2 (M= Yb, Sc, Eu, Y, Lu and Gd). *Vacuum*, *212*, 112011.

[3] Bonnet, J. E., & Daou, J. N. (1977). Rare-earth dihydride compounds: Lattice thermal expansion and investigation of the thermal dissociation. Journal of Applied Physics, 48(3), 964-968.

[4] Pebler, A., & Wallace, W. E. (1962). Crystal structures of some lanthanide hydrides1. *The Journal of Physical Chemistry*, *66*(1), 148-151.

[5] Baba Arabi, N. E. (2023). Contribution to the study of the physical properties of thulium dihydride TmH_2 using density functional theory (DFT) [Master's thesis, Kasdi Merbah University, Ouargla, Algeria].

[6] Jaroń, T., Ying, J., Tkacz, M., Grzelak, A., Prakapenka, V. B., Struzhkin, V. V., & Grochala, W. (2022). Synthesis, structure, and electric conductivity of higher hydrides of ytterbium at high pressure. *Inorganic Chemistry*, *61*(23), 8694-8702.

[7] Ayat, H., & Ben Aoun, D. (2022). Study of the properties of rubidium dihydride using density functional theory. Kasdi Merbah University – Ouargla.

[8] Benali, K. (2021). Study of the properties of gadolinium dihydride using density functional theory. University of Kasdi Merbah – Ouargla. (Master thesis).

[9] Ao, B. Y., Wang, X. L., Shi, P., Chen, P. H., Ye, X. Q., Lai, X. C., ... & Gao, T. (2012). Lattice contraction of cerium hydrides from first-principles LDA+ U calculations. *International journal of hydrogen energy*, *37*(6), 5108-5113.

[10] Ao, B. Y., Shi, P., Guo, Y., & Gao, T. (2013). The abnormal lattice contraction of plutonium hydrides studied by first-principles calculations. *Chinese Physics B*, *22*(3), 037103.

[11] Bousahla, M. N., Bousahla, M. A., Chahed, A., Bousahla, Z., Rozale, H., & Bendjilali, H. (2023). Structural, Mechanical, Elastic, Electronic, Magnetic and Optical Properties of Spinel

Compounds ATi2S4 (A= Ca, Sr and Ba): AB Initio Study. *Annals of the West University of Timisoara. Physics Series*, *65*(1), 21-40.

[12] BYJU'S. (n.d.). What are energy bands [Photograph]. Retrieved June 24, 2025, from https://byjus.com/physics/what-are-energy-bands/

[13] Geek3. (2008, December 6). Brillouin Zone (1st, FCC) Wikimedia Commons.

[14] ChemistryStudent.com. (n.d.). d-orbital splitting Retrieved June 24, 2025,

[15] Capecchi, D., & Ruta, G. (2015). Strength of materials and theory of elasticity in 19th century Italy. *Springer*.

[16] Shadley, J. R. (1968). Stresses and displacements in thick layer containing an axially symmetrical Dugdale crack.

[17] Daniel, I. M. (2002). Recent advances in experimental mechanics: in honor of Isaac M. Daniel.

[18] Kube, C. M. (2016). Elastic anisotropy of crystals. *AIP advances*, *6*(9).

[19] Katz, J. L., & Meunier, A. (1987). The elastic anisotropy of bone. *Journal of biomechanics*, *20*(11-12), 1063-1070.

[20] Benjamina, U. S., Tamunobereton-ari, I., Opiriyaboa, H. I., & Mogaba, P. (2022). Comparative Analysis Of Static Shear Modulus And Dynamic Shear Modulus Determined By Geophysical And Geotechnical Investigation. *Earth Sciences Malaysia (ESMY)*, *6*(1), 01-10.

[21] Hill, R. (1952). The elastic behaviour of a crystalline aggregate. *Proceedings of the Physical Society. Section A*, *65*(5), 349.

[22] Man, C. S., & Huang, M. (2011). A simple explicit formula for the Voigt-Reuss-Hill average of elastic polycrystals with arbitrary crystal and texture symmetries. *Journal of Elasticity*, *105*(1), 29-48.

[23] Callister Jr, W. D., & Rethwisch, D. G. (2020). *Materials science and engineering: an introduction*. John wiley & sons.

[24] Imran, A. (2025). Computational Investigation of Mechanical properties in multi-materials produced by Additive.

[25] Kasala, S. (2018). Recycled technical plastics as raw material for plastics and composite products.

[26] Chen, X. Q., Niu, H., Li, D., & Li, Y. (2011). Modeling hardness of polycrystalline materials and bulk metallic glasses. *Intermetallics*, *19*(9), 1275-1281.

[27] Tian, Y., Xu, B., & Zhao, Z. (2012). Microscopic theory of hardness and design of novel superhard crystals. Acta Materialia, 60(13–14), 5380–5392.

[28] Saidi, F., Mokhdar, S., Dergal, M., Mahmoudi, A., Kallekh, A., & Abd El-Gawad, H. H. (2023). Ab initio study of the structural, electronic, magnetic, mechanical, optical, and dynamical properties of the rare-earth dihydrides MH2 (M= Yb, Sc, Eu, Y, Lu and Gd). *Vacuum*, *212*, 112011.

[29] Saidi, F., Mokhdar, S., Dergal, M., Mahmoudi, A., Kallekh, A., & Abd El-Gawad, H. H. (2023). Ab initio study of the structural, electronic, magnetic, mechanical, optical, and dynamical properties of the rare-earth dihydrides MH2 (M= Yb, Sc, Eu, Y, Lu and Gd). *Vacuum*, *212*, 112011.

[30] Pugh, S. F. (1954). XCII. Relations between the elastic moduli and the plastic properties of polycrystalline pure metals. *The London, Edinburgh, and Dublin Philosophical Magazine and Journal of Science*, *45*(367), 823-843.

[31] Pettifor, D. G. (1984). A chemical scale for crystal-structure maps. *Solid State Communications*, *51*(1), 31-34.

[32] Anderson, O. L. (1963). A simplified method for calculating the Debye temperature from elastic constants. *Journal of Physics and Chemistry of Solids*, *24*(7), 909-917.

[33] Anderson, O. L. (1995). *Equations of state of solids for geophysics and ceramic science* (No. 31). Oxford university press.

[34] Mouhat, F., & Coudert, F. X. (2014). Necessary and sufficient elastic stability conditions in various crystal systems. *Physical review B*, *90*(22), 224104.

[35] Fine, M. E., Brown, L. D., & Marcus, H. L. (1984). Elastic constants versus melting temperature in metals. *Scripta metallurgica*, *18*(9), 951-956.

[36] Linderborg, O. H. (2025). *Socrates and his Demise: An Examination of the Historical Figure*. Taylor & Francis.

[37] Fox, M. (2010). *Optical properties of solids* (Vol. 3). Oxford university press.

[38] Dresselhaus, M., Dresselhaus, G., Cronin, S., Gomes Souza Filho, A., Dresselhaus, M., Dresselhaus, G., ... & Gomes Souza Filho, A. (2018). Optical Properties of Solids over a Wide Frequency Range. *Solid State Properties: From Bulk to Nano*, 391-410.

[39] Lee, G., Yu, E. S., Ryu, Y. S., & Seo, M. (2022). The perspectives of broadband metasurfaces and photo-electric tweezer applications. *Nanophotonics*, *11*(9), 1783-1808.

General Conclusion

General Conclusion

In this work, we investigated the physical properties of lutetium dihydride (LuH_2) using Density Functional Theory (DFT) within the Generalized Gradient Approximation (GGA), employing the WIEN2k simulation package and the plane-wave method. The study encompassed structural, energetic, electronic, thermodynamic, and optical properties to evaluate the behavior of LuH_2 and its potential technological applications.

The structural analysis showed good agreement with previously reported results, particularly regarding the lattice constant, equilibrium volume, and bulk modulus, confirming the reliability of the adopted computational model. The negative values of formation energy, cohesive energy, and hydrogen binding energy indicate that the compound is thermodynamically stable and can be synthesized experimentally.

Electronic analysis revealed a clear metallic nature, with evident hybridization between the atomic orbitals of hydrogen and lutetium. Near the Fermi level, the contribution of lutetium orbitals is dominant, while that of hydrogen is minimal, consistent with the typical behavior of metal hydrides.

Regarding the optical properties, we calculated the real and imaginary parts of the dielectric function, refractive index, absorption coefficient, reflectivity, and optical conductivity over an energy range up to 14 eV. The first absorption peak was found within the visible range (violet light), while the remaining peaks lie in the ultraviolet region, suggesting that LuH_2 can serve as an effective UV optical filter.

Based on these findings, we conclude that lutetium dihydride exhibits promising characteristics for applications in optics and hydrogen storage technologies. Future studies may explore the effects of external factors such as pressure and temperature, or investigate similar compounds within the same family, to deepen our understanding of metal hydrides and their technological potential.

الملخص:

يُعد الهيدروجين خيارًا واعدًا للطاقة المستقبلية، وتخزينه يمثل تحديًا رئيسيًا. في هذا العمل، درسنا خصائص ثنائي هيدريد اللوتيتيوم LuH_2 باستخدام برنامج wien2k المعتمد على نظرية دالية الكثافة (DFT) وتقريب GGA. أظهرت النتائج أن للمركب طابعًا معدنيًا وثباتًا طاقويًا جيدًا، مع استجابة بصرية في مجال الأشعة فوق البنفسجية، مما يجعله مناسبًا للتطبيقات البصرية وتخزين الهيدروجين.

كلمات مفتاحية: ثنائي هيدريد اللوتيتيوم، DFT، wien2k، GGA.

Abstract:

Hydrogen is a promising candidate for future energy. This work investigates the properties of lutetium dihydride (LuH_2) using wien2k based on DFT and GGA. The compound shows energetic stability, metallic and brittle behavior, making it suitable for hydrogen storage and optical applications.

Keywords: lutetium dihydride, DFT, wien2k, GGA.

Résumé :

L'hydrogène est une solution prometteuse pour l'énergie future. Nous avons étudié les propriétés du dihydrure de lutécium (LuH_2) en utilisant wien2k basé sur la DFT et l'approximation GGA. Les résultats montrent une stabilité énergétique, un caractère métallique, et une réponse optique dans l'UV, suggérant son utilité dans le stockage de l'hydrogène et les applications optiques.